Article

Cell Reports

APache Is an AP2-Interacting Protein Involved in Synaptic Vesicle Trafficking and Neuronal Development

Graphical Abstract

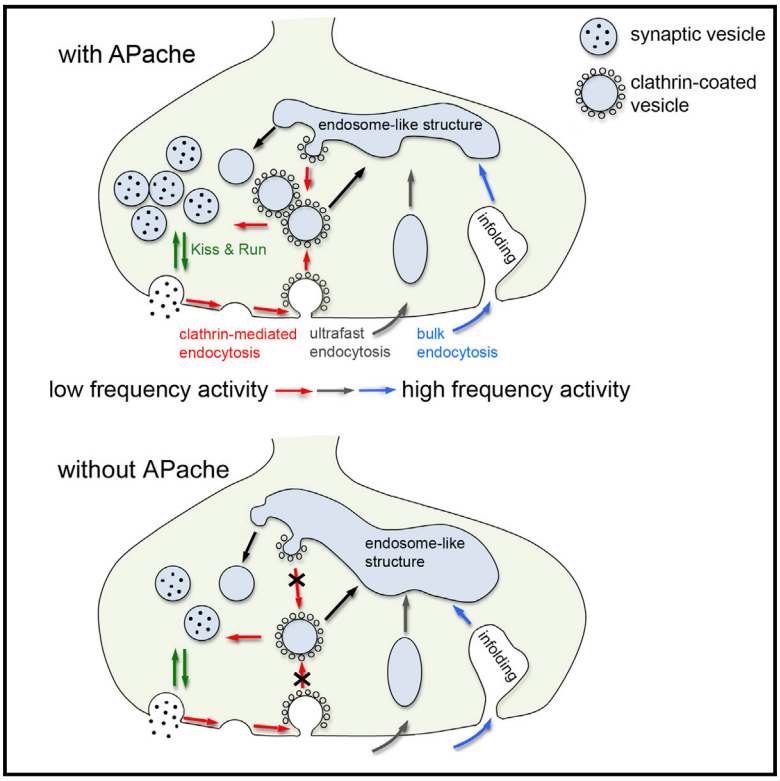

Highlights

- APache is a presynaptic AP2 interactor on clathrin-coated vesicles
- APache silencing affects the early neuronal development *in vitro* and *in vivo*
- APache-silenced synapses exhibit a marked endocytic phenotype
- APache silencing impairs clathrin-mediated endocytosis and synaptic function

Authors

Alessandra Piccini, Enrico Castroflorio, Pierluigi Valente, ..., Flavia Valtorta, Fabio Benfenati, Silvia Giovedì

Correspondence

fabio.benfenati@iit.it (F.B.), silvia.giovedi@unige.it (S.G.)

In Brief

Piccini et al. uncovered the AP2-interacting protein APache that acts in the clathrin-mediated endocytic machinery and synaptic vesicle trafficking. They found that silencing APache impairs neuronal development and neurotransmitter release during repetitive stimulation by markedly reducing vesicle recycling.

Piccini et al., 2017, Cell Reports *21*, 3596–3611
December 19, 2017
https://doi.org/10.1016/j.celrep.2017.11.073

CellPress

OPEN ACCESS
CellPress

Cell Reports
Article

APache Is an AP2-Interacting Protein Involved in Synaptic Vesicle Trafficking and Neuronal Development

Alessandra Piccini,[1] Enrico Castroflorio,[2] Pierluigi Valente,[1] Fabrizia C. Guarnieri,[3] Davide Aprile,[1] Caterina Michetti,[2] Mattia Bramini,[2] Giorgia Giansante,[1] Bruno Pinto,[4,5] Annalisa Savardi,[1,4] Fabrizia Cesca,[2] Angela Bachi,[6] Angela Cattaneo,[6] Jonathan D. Wren,[7] Anna Fassio,[1,2] Flavia Valtorta,[3] Fabio Benfenati,[1,2,8,*] and Silvia Giovedì[1,8,9,*]

[1]Department of Experimental Medicine, University of Genova, 16132 Genova, Italy
[2]Center for Synaptic Neuroscience and Technology, Istituto Italiano di Tecnologia, 16132 Genova, Italy
[3]San Raffaele Scientific Institute and Vita Salute University, 20132 Milano, Italy
[4]Local Micro-environment and Brain Development Laboratory, Istituto Italiano di Tecnologia, 16163 Genova, Italy
[5]Bio@SNS, Scuola Normale Superiore, 56126 Pisa, Italy
[6]IFOM, FIRC Institute of Molecular Oncology, 20132 Milano, Italy
[7]Department of Arthritis and Clinical Immunology, Oklahoma Medical Research Foundation, Oklahoma City, OK 73104-5005, USA
[8]These authors contributed equally
[9]Lead Contact
*Correspondence: fabio.benfenati@iit.it (F.B.), silvia.giovedi@unige.it (S.G.)
https://doi.org/10.1016/j.celrep.2017.11.073

SUMMARY

Synaptic transmission is critically dependent on synaptic vesicle (SV) recycling. Although the precise mechanisms of SV retrieval are still debated, it is widely accepted that a fundamental role is played by clathrin-mediated endocytosis, a form of endocytosis that capitalizes on the clathrin/adaptor protein complex 2 (AP2) coat and several accessory factors. Here, we show that the previously uncharacterized protein KIAA1107, predicted by bioinformatics analysis to be involved in the SV cycle, is an AP2-interacting clathrin-endocytosis protein (APache). We found that APache is highly enriched in the CNS and is associated with clathrin-coated vesicles via interaction with AP2. APache-silenced neurons exhibit a severe impairment of maturation at early developmental stages, reduced SV density, enlarged endosome-like structures, and defects in synaptic transmission, consistent with an impaired clathrin/AP2-mediated SV recycling. Our data implicate APache as an actor in the complex regulation of SV trafficking, neuronal development, and synaptic plasticity.

INTRODUCTION

High-frequency and sustained neurotransmitter release is dependent on the correct reformation of exocytosed synaptic vesicles (SVs) by efficient endocytosis. During physiological activity, clathrin-mediated endocytosis (CME) represents the best-characterized pathway for recycling of fully fused SVs (Heuser and Reese, 1973; Granseth et al., 2006; Dittman and Ryan, 2009; Saheki and De Camilli, 2012), although the precise mechanisms of SV membrane retrieval and functional SV reconstitution remain highly controversial (Soykan et al., 2016; Cousin, 2017).

At the plasma membrane, the most abundant adaptor coordinating coat recruitment and cargo selection into endocytic pits is the heterotetrameric adaptor protein complex 2 (AP2), comprised of two large α and β2 subunits, a medium-size μ2 subunit, and a small δ2 subunit. Among the numerous accessory proteins believed to control the internalization pathway (Slepnev and De Camilli, 2000), clathrin and AP2 constitute the two main protein interaction hubs, around which an extensive and highly dynamic endocytic network is organized to achieve clathrin-coated vesicle (CCV) formation (Schmid and McMahon, 2007). However, other alternate clathrin-associated sorting proteins (CLASP) have recently been identified for the internalization of selected cargo membrane proteins (Traub and Bonifacino, 2013). Thus, synapses have evolved distinct mechanisms to maintain membrane homeostasis and the dominant mode for SV recycling may depend on the type of neuron and its activity pattern (Valtorta et al., 2001; Kononenko and Haucke, 2015; Park et al., 2016). Despite intense research, much remains to be learned about the exact molecular components of the endocytic pathways.

Here, we characterize the highly conserved AP2-interacting clathrin-endocytosis protein APache (NP_001007575.2) and investigate its physiological role in neuronal development and synaptic function. APache is a neuron-specific protein, expressed in axonal processes and presynaptic terminals, that specifically interacts with AP2 on CCVs. Our data indicate that APache plays a role in neuronal development and is required to maintain normal SV recycling in mature neurons. APache can thus be considered an important actor of the clathrin-mediated endocytic machinery at the synapse that is required for normal synaptic transmission.

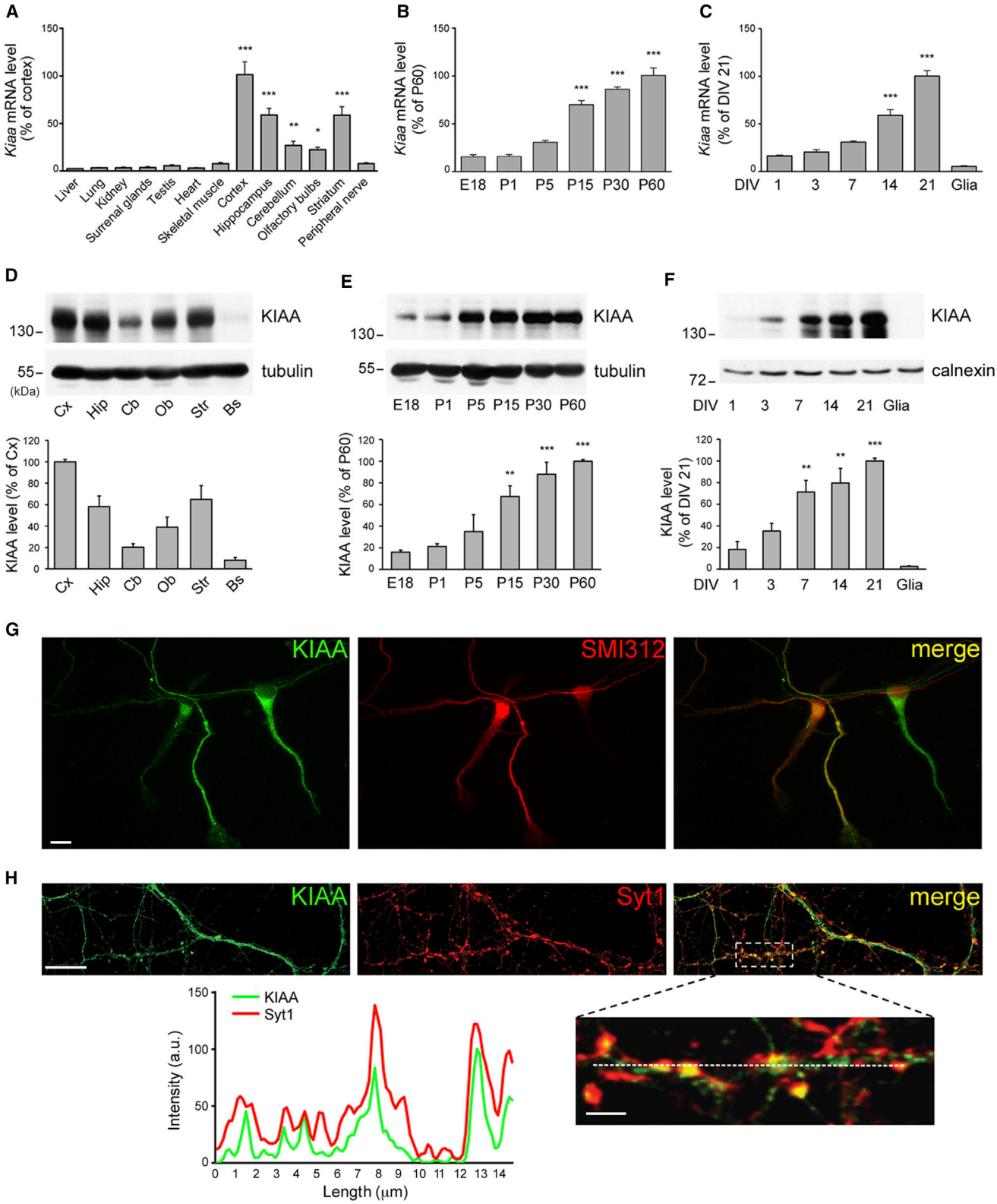

Figure 1. Expression and Localization of Endogenous KIAA1107 in Neurons

(A) Real-time PCR analysis of *Kiaa1107* mRNA levels in various mouse tissues. Means ± SEM of n = 3 animals; one-way ANOVA/Bonferroni's multiple comparison test; *p < 0.05; **p < 0.01; ***p < 0.001 versus liver.

(legend continued on next page)

RESULTS

Identification of KIAA1107 by GAMMA

Global Microarray Meta-Analysis (GAMMA) is a program previously developed to identify highly correlated transcripts within microarray experiments, which can then be used to infer function, phenotype, genetic network, and disease relevance for uncharacterized genes (Wren, 2009). GAMMA was used to search for uncharacterized genes associated with SV recycling, and KIAA1107 was the highest scoring gene without prior publications. The predicted phenotypes associated with KIAA1107 disruption, predicted disease relevance, and predicted cellular/anatomical structures of relevance to KIAA1107 activity are shown in Figure S1.

KIAA1107 is evolutionarily conserved from zebrafish to human. The murine *Kiaa1107* gene (official symbol: A830010M20Rik) is located on chromosome 5 (forward strand). According to the Ensembl database, the gene gives rise to five differentially spliced transcripts, four of which are predicted to be protein coding. Conversely, the NCBI database includes only two splicing variants (NCBI Refseq NM_001007574.2 and NM_001168557.1, corresponding to ENSMUST00000112671.8 and ENSMUST00000060553.7, respectively, in the Ensembl database). Among these two, one transcript codes for a protein of 1,088 amino acids (aas) and is considered the main isoform, whereas the other codes for a smaller protein of 443 aas. We cloned the major isoform, with an expected molecular mass of 117 kDa, and will refer to it as KIAA1107 throughout. No significant similarity with other proteins could be identified with a BLAST search of the murine KIAA1107 against the *Mus musculus* RefSeq protein database. No conserved protein domains were predicted using bioinformatics tools, such as SMART and InterProScan, but one coiled-coil region was predicted at aa position 820–841 with COILS2 (probability 62.9% with window 21; MTIDK matrix; no weights). Hence, the sequence of KIAA1107 does not reveal any particular information about its possible function or localization, but the GAMMA predictions on its involvement in synaptic function were really strong and persuaded us to investigate it further.

To characterize KIAA1107, we first generated a polyclonal antibody directed against a conserved region comprising aas 732–894 of the mouse ortholog (Figure S2A). The affinity-purified antibody recognized both overexpressed and endogenous KIAA1107 as a band of ~140 kDa in immunoblotting assays (Figures S2B and S2C). Its specificity was further proved by preadsorbing the primary antibody with a molar excess of the recombinant immunizing peptide (Figure S2D).

To silence KIAA1107 expression, we designed 3 short hairpin RNAs (shRNAs) based on the coding sequence (shRNA#1) and the 3′ UTR (shRNA#2 and #3) of the mouse *Kiaa1107* transcript, inserted them into a bicistronic lentiviral vector expressing the fluorescent reporter mCherry, and validated their specificity and efficacy by immunoblotting (Figures S2B and S2C). shRNA#2 was chosen for the subsequent studies, being the most active in knocking down the endogenous KIAA1107 expression. The specificity of the KIAA1107 antibody was subsequently demonstrated by immunocytochemistry of silenced neurons (Figure S2E).

KIAA1107 Is a Neuron-Specific and Developmentally Regulated Protein

We evaluated *Kiaa1107* mRNA and protein levels in various tissues and brain areas of adult mice and determined its developmental expression profile in the intact mouse cortex and primary neuronal cultures (Figures 1A–1F). KIAA1107 was primarily expressed in brain, with the highest mRNA and protein levels in the cerebral cortex, hippocampus, and striatum (Figures 1A and 1D). It was already present in the mouse brain at prenatal and early postnatal stages (embryonic day 18 [E18]–postnatal day 5 [P5]), and its expression increased during postnatal development to reach a plateau at 1 month of age (Figures 1B and 1E). A similar pattern was reproduced in primary cortical neurons, where *Kiaa1107* mRNA and protein levels were discernible at early stages of development (1–3 days in vitro [DIV]) and were greatly enhanced between 7 and 21 DIV (Figures 1C and 1F). Consistent with the strictly neuron-specific expression of the protein, KIAA1107 was not detected in primary astroglial cultures.

To examine the localization of KIAA1107 in neurons during development, 5 and 17 DIV primary cortical neurons were analyzed by immunocytochemistry. In early stages of *in vitro* development, KIAA1107 was expressed in the cell body and growing processes, including the axon, as shown by the colocalization with the pan-axonal neurofilament marker SMI312

(B) Real-time PCR analysis of *Kiaa1107* mRNA expression in the cerebral cortex of developing mice (from embryonic day 18 [E18] to postnatal day 60 [P60]). Means ± SEM of n = 3 animals/developmental stage; one-way ANOVA/Bonferroni's multiple comparison test; ***p < 0.001 versus E18.

(C) Real-time PCR analysis of *Kiaa1107* mRNA expression in primary cultures of cortical neurons at various stages of development (from 1 to 21 DIV). Means ± SEM of n = 3 independent cultures/developmental stage; one-way ANOVA/Bonferroni's multiple comparison test; ***p < 0.001 versus DIV 1.

(D) Regional expression of KIAA1107 in the adult mouse brain. Representative immunoblot (top) and relative densitometric quantification normalized on βIII tubulin levels (bottom) are shown. Means ± SEM of n = 4 animals. Bs, brain stem; Cb, cerebellum; Cx, cortex; Hip, hippocampus; Ob, olfactory bulb; Str, striatum.

(E) Temporal expression profile of KIAA1107 in the developing mouse cerebral cortex (from E18 to P60). Representative immunoblot of KIAA1107 levels (top) and relative densitometric quantification normalized on βIII tubulin (bottom) are shown. Means ± SEM of n = 3 animals/developmental stage; one-way ANOVA/Bonferroni's multiple comparison test; **p < 0.01; ***p < 0.001 versus E18.

(F) Temporal expression profile of KIAA1107 in primary cortical neurons at various stages of development (from 1 to 21 DIV). Representative immunoblot of KIAA1107 levels (top) and relative densitometric quantification normalized on calnexin (bottom) are shown. Means ± SEM of n = 3 independent neuronal cultures/developmental stage; one-way ANOVA/Bonferroni's multiple comparison test; **p < 0.01; ***p < 0.001 versus DIV 1.

(G and H) Localization of KIAA1107 in cultured neurons during development. Representative images of cortical neurons fixed and double stained for KIAA1107 (green) and SMI312 (red) at 5 DIV (G) or for KIAA1107 (green) and synaptotagmin-1 (Syt1) (red) at 17 DIV (H) are shown. The scale bars represent 10 μm. In the bottom panel, linear intensity profiles of KIAA1107 (green) and Syt1 (red) fluorescence (measured along the dashed lines as indicated in the merge field) illustrate the presynaptic localization of KIAA1107 in mature neurons. The scale bar represents 2 μm.

See also Figures S1 and S2.

(Figure 1G). In mature neurons, the antibody also revealed a punctate nerve terminal pattern that partially colocalized with the presynaptic marker synaptotagmin-1 (Figure 1H). These data indicate that KIAA1107 is a developmentally regulated, widely expressed neuron-specific protein, mainly present at axonal and presynaptic terminal levels.

KIAA1107 Is an AP2 Interactor

In order to identify KIAA1107 protein-interacting partners, we employed a mass spectrometry (MS) approach using FLAG-KIAA1107, purified from SH-SY5Y human neuroblastoma or COS-7 cells, as a bait to pull-down KIAA1107 interactors from SH-SY5Y cell or subcellular fractions of mouse brain extracts (Figure 2A). The bands of interest were excised from the Coomassie-blue-stained gels, analyzed by liquid chromatography (LC)-MS/MS, and the MS/MS spectra were assigned to peptides with a >95% confidence level. In two independent preparations, a total of 163 proteins were reproducibly identified as specific KIAA1107-binding partners (MSdataSHSY5Y_XTandem.sf3 and MSdataCOS7_XTandem.sf3 in Data S1), seven of which resulted to be in common between the human and murine cellular models (Figure 2B). These included AP2 (α1 and β subunits) and AP3 (β2 and δ1 subunits) found in CCVs that traffic cargoes from the plasma membrane and between the endosomal and lysosomal systems, respectively (Robinson, 2004); Numb-like protein (NUMBL) involved in neural development and clathrin-dependent endocytosis (Sestan et al., 1999; Nishimura et al., 2003; Santolini et al., 2000); Bcl-2-associated transcription factor that interacts with antiapoptotic members of the Bcl-2 family (Kasof et al., 1999); V-type proton ATPase catalytic subunit A, a component of vacuolar ATPase (van Hille et al., 1993); and dynactin subunit1 (DCTN1) involved in organelle transport (Schroer, 2004).

We first focused our attention on AP2, the main adaptor protein responsible for CME (Conner and Schmid, 2003) and proceeded to co-immunoprecipitation assays to validate the potential interaction with KIAA1107. After verifying by MS analysis that the ~140-kDa protein band immunoprecipitated from mouse brain extract with the KIAA1107 polyclonal antibody was indeed the endogenous 1,088-aa KIAA1107 isoform, we found that both AP2 α and β subunits were specifically co-immunoprecipitated with endogenous KIAA1107 from mouse brain extracts (Figure 2C), whereas no interaction of KIAA1107 with clathrin was observed under the same conditions in which the AP2/clathrin binding was evident (Figure 2D). Interestingly, KIAA1107 was also co-immunoprecipitated from mouse brain extracts with anti-AP2α antibodies (Figure 2D), demonstrating the reciprocity of the interaction between KIAA1107 and AP2.

To restrict the part of the protein that interacts with AP2, we performed additional pull-down assays in mouse brain extracts using FLAG-KIAA1107 full-length, N- and C-terminal fragments. Interestingly, AP2α and AP2β were affinity purified only by the N-terminal fragment, whereas no interactions were observed with the C-terminal fragment (Figures S3A and S3B). In addition, the possibility of a nonspecific immunoprecipitation of AP2 was excluded by performing analogous co-immunoprecipitation assays in mouse liver extracts, a tissue that expresses AP2, but not KIAA1107 (Figure S3C).

We then combined the KIAA1107 binding proteins detected in our study with the results of another large proteomic study (Hein et al., 2015) that also identified KIAA1107 as a potential NUMBL interactor. Thus, we searched for additional shared interactions and overlaps with genes that GAMMA predicted to be relevant to KIAA1107 to infer a potential genetic neighborhood for KIAA1107 (Figure 2E). Such a predictive study revealed connections between KIAA1107 and clusters of genes playing key roles in exocytosis (SNAP25, syntaxin, syntaxin-binding protein, VAMP, NSF, and synaptotagmin-1), endocytosis (dynamin1, AP2, AP3, and Eps15), and neuronal development (Notch1, NUMB, and NUMBL).

KIAA1107 Is Expressed at Nerve Terminals and Associates with CCVs

As AP2 is one of the major coat proteins of CCVs, it was important to determine whether KIAA1107 is associated with CCVs. We isolated a CCV-enriched fraction from cultured rat neurons, successively stripped it and analyzed by immunoblotting the various fractions. The CCV preparation was highly enriched in the coat proteins clathrin and AP2, which were efficiently stripped from the purified vesicles, and in the integral vesicle membrane proteins synaptotagmin-1 and synaptophysin, which were not stripped (Figure 3A). In contrast, an accessory protein of CME, such as dynamin, was neither enriched on CCVs nor stripped, indicating that it does not function as classical clathrin adaptor (Slepnev and De Camilli, 2000). KIAA1107 was significantly enriched in the CCV fraction, although to a lesser extent than clathrin, and could be stripped by treatment with Tris buffer (Figure 3A). These data show that KIAA1107 is a protein associated with the coat component and not with the vesicle fraction.

In subcellular fractions prepared from rat forebrain, KIAA1107 immunoreactivity was mostly associated with the S2 fraction, consistent with the widespread localization of the protein in neurons (Figure 3B). However, it co-enriched with AP2 in the nerve-terminal-derived fractions LS1 and LP2, containing SVs and endosomal membranes, and its distribution roughly paralleled that of AP2 in other fractions (Figure 3B). Consistent with the biochemical data, a close colocalization of endogenous KIAA1107 with the essential components of the endocytic machinery AP2 and dynamin1 was observed in primary cortical neurons (17 DIV; Figure 3C). Notably, dynamin1 was identified as an indirect KIAA1107 interactor in a recent proteomics study (Gorini et al., 2010). These data suggest that KIAA1107 is closely associated with intracellular vesicular structures and binds specifically to AP2 on CCVs.

KIAA1107 Silencing Affects the Early Neuronal Development

CME controls cell surface expression of receptors, including those for axon guidance cues (Tojima et al., 2010), and AP2 plays a key role in directed cell migration (Raman et al., 2014). To interrogate the role of KIAA1107 in neuronal development, we acutely downregulated KIAA1107 expression in primary cortical neurons by RNAi with KIAA1107 shRNA#2

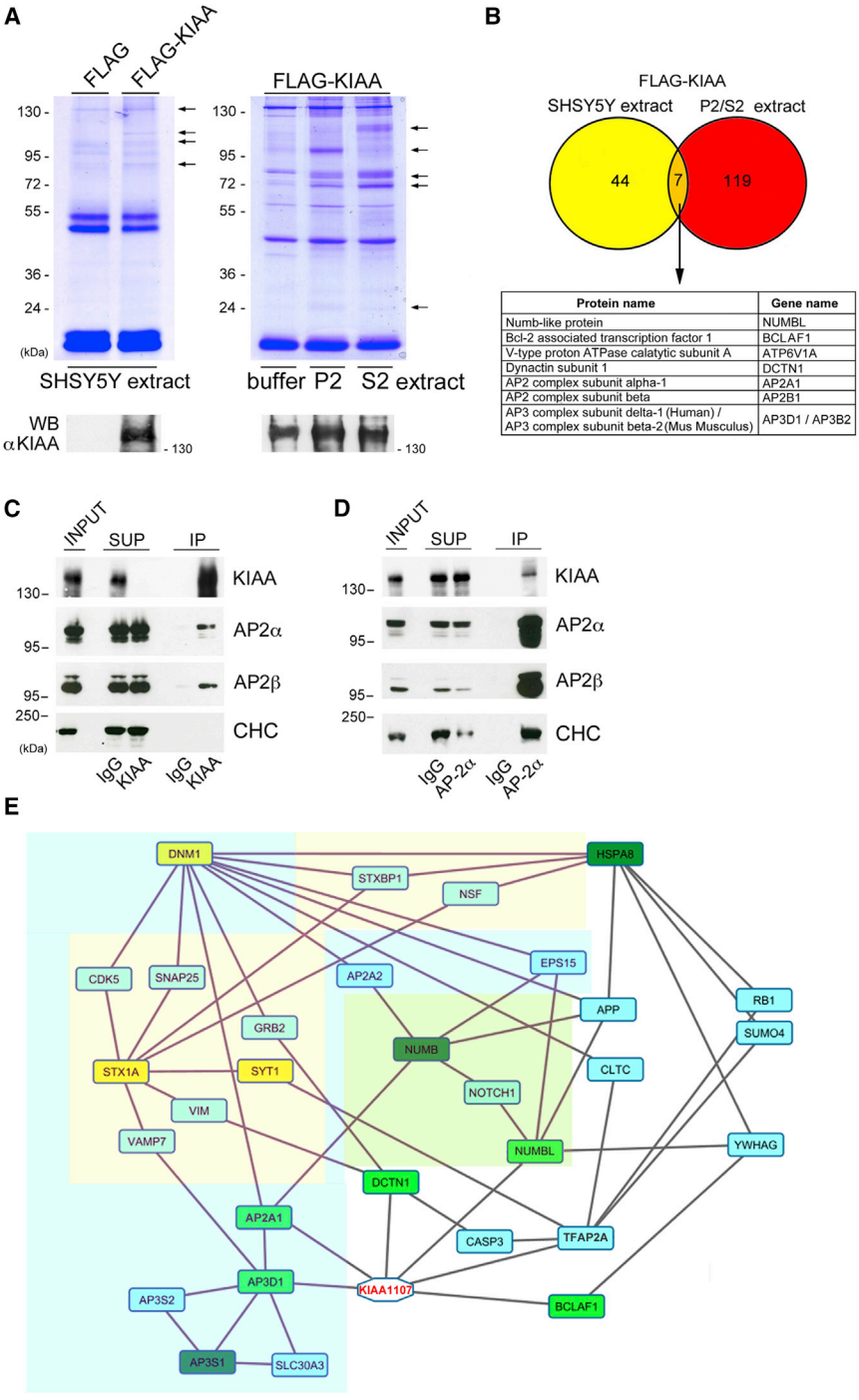

Figure 2. Identification of AP2 as a Specific KIAA1107 Interactor

(A and B) MS analysis of KIAA1107 interactors.

(A, top) Coomassie blue stained SDS-PAGE gels for proteins affinity purified by pull-down with overexpressed FLAG-KIAA1107 or FLAG-control in extracts of either SH-SY5Y cells (left panel) or subcellular fractions of mouse brain (cytosolic/microsomal S2 fraction or synaptosomal P2 fraction; right panel) are shown. Selected gel bands (arrows) were excised from the gels and analyzed by LC-MS/MS. (Bottom) KIAA1107 expression and specific precipitation in the samples was confirmed by western blotting (WB). The procedure was repeated twice with independent preparations.

(B) Venn diagram of the number of proteins identified by LC-MS/MS analysis exclusively in FLAG-KIAA1107 samples. The result showed 7 proteins (orange area) shared by both experimental models (protein and gene names are listed in the table) within 44 (yellow area) and 119 (red area) specific proteins for SH-SY5Y cells and mouse brain, respectively.

(C and D) Co-immunoprecipitation of KIAA1107 and AP2. Mouse brain extracts were subjected to immunoprecipitation (IP) with anti-KIAA1107 polyclonal antibodies (C), anti-AP2α monoclonal antibodies (D), or control immunoglobulin Gs (IgGs). Equal aliquots (2% of total) of the starting material (INPUT) and the supernatants (SUP) together with the IP samples were subjected to immunoblotting with the indicated antibodies (CHC [clathrin heavy chain]). The same membranes were stripped and re-probed for AP2α and β. The IPs were performed three times with similar results.

(E) Putative KIAA1107 genetic neighborhood based upon protein-protein interactions (PPIs). Our data (light green) were combined with PPIs found in a large proteomics study by Hein et al. (2015; dark green). Then, we searched for their shared PPIs (blue), as documented in Entrez Gene, and looked for overlap with GAMMA-predicted genes that fit into this network (yellow) to infer a potential genetic neighborhood for KIAA1107. Exocytic (yellow area), endocytic (blue area), and developmental (green area) clusters of genes are highlighted.

See also Figure S3 and Data S1.

(Figure S4). Cell morphology analysis revealed that silenced neurons displayed a significant impairment in neuronal development in terms of neurite number and length at early stages *in vitro* (3 and 5 DIV) compared to cells treated with control shRNA (shRNActr) (Figures 4A–4C). Interestingly, silenced neurons also showed a reduced expression level of AP2 (Figure S4), potentially due to partial degradation of the protein in the absence of complex formation with KIAA1107. The defective neurite outgrowth was completely rescued by the expression of EGFP-KIAA1107, a construct intrinsically resistant to shRNA#2 (Figures 4A–4C), indicating that the developmental impairment was specifically due to the downregulation of endogenous KIAA1107 and not to shRNA-mediated off-target effects. Moreover, KIAA1107 overexpression per se did not affect neuronal maturation, as length and number of processes did not differ between control and EGFP-KIAA1107-overexpressing neurons at both 3 and 5 DIV.

To further investigate the role of KIAA1107 in neocortical development *in vivo*, we downregulated its expression by in

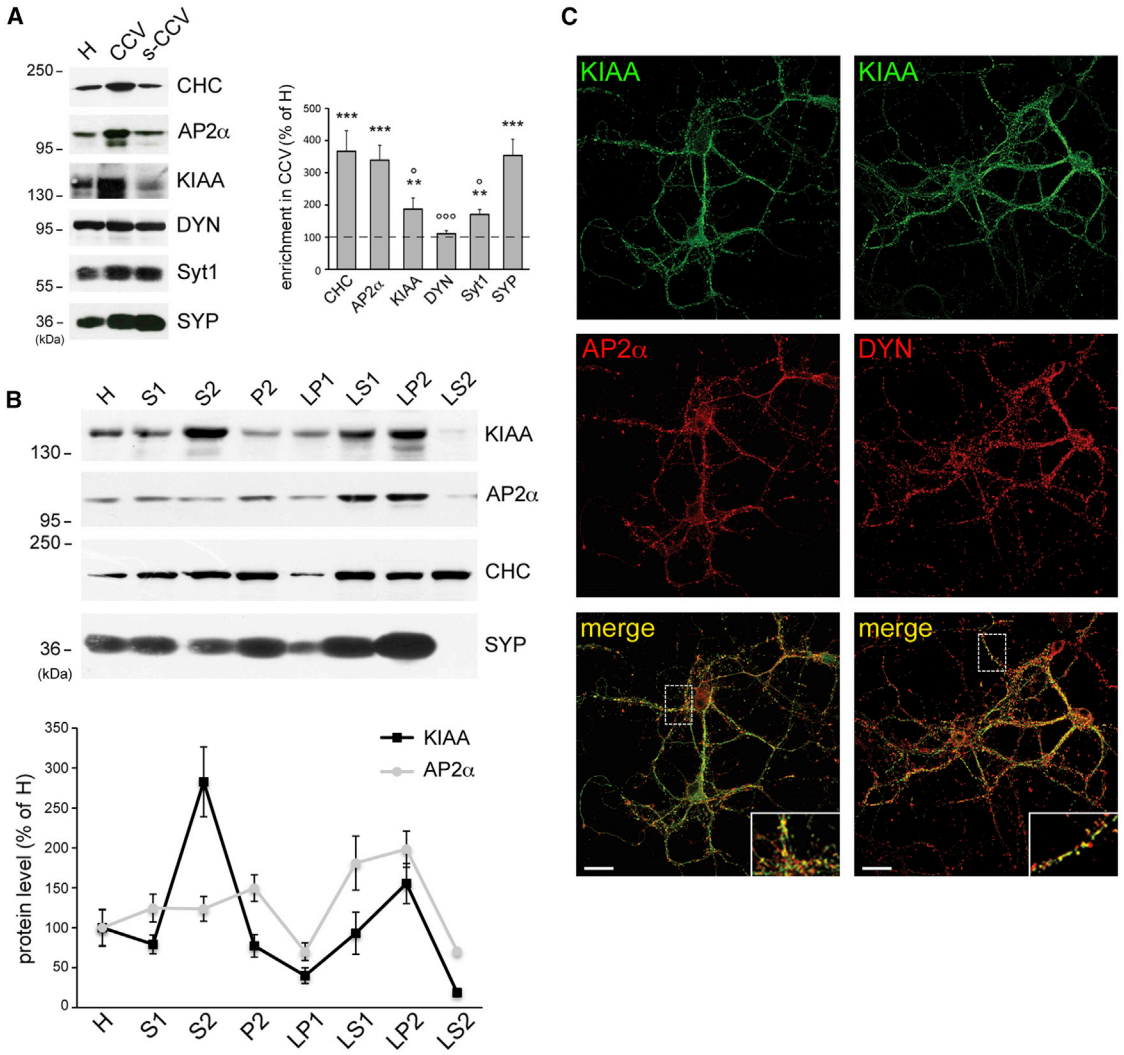

Figure 3. KIAA1107 Is a CCV-Associated Protein

(A) KIAA1107 is enriched in CCVs. (Left) The distribution of KIAA1107 immunoreactivity is compared with that of components of clathrin coats (CHC and AP2α), SVs (Syt1 and synaptophysin [SYP]), and CCV accessory proteins (dynamin1 [DYN]). Representative immunoblots are shown. Equal amounts of protein were loaded. H, total homogenate; s-CCV, stripped-CCV. (Right) Densitometric quantification of protein levels in the CCV-enriched fraction expressed as mean (±SEM) percentages of H is shown (n = 3 independent experiments); $^{**}p < 0.01$, $^{***}p < 0.001$ versus H, unpaired Student's t test; $^{\circ}p < 0.05$, $^{\circ\circ\circ}p < 0.001$ versus CHC, one-way ANOVA/Bonferroni's multiple comparison test.

(B) KIAA1107 co-fractionates with AP2. (Top) Subcellular fractions of rat forebrain were analyzed by immunoblotting using KIAA1107, AP2α, and CHC antibodies. The distribution of the specific SV marker SYP in the same fractions is shown for comparison. LP1, crude synaptic plasma membranes; LP2, crude SVs; LS1, SV-enriched supernatant fraction; LS2, synaptosol; P2, crude synaptosomes; S1, post-nuclear supernatant; S2, cytosolic and microsomal fraction. (Bottom) Densitometric quantification of KIAA1107 and AP2α immunoreactivities in the various subcellular fractions is shown. Data are expressed in percent of the relative H value (means ± SEM of n = 4 independent experiments).

(C) KIAA1107 colocalizes with the endocytic network. Representative confocal images of mature cortical neurons (17 DIV) double stained for KIAA1107 (green) and AP2α (red, left panels) or dynamin1 (DYN) (red, right panels) showing a largely overlapping staining of the proteins (magnified in the insets) are shown. The scale bars represent 10 μm (4.2 μm in the insets). Pearson's correlation coefficient is 0.846 ± 0.041 and 0.796 ± 0.039 for KIAA1107/AP2α and KIAA1107/DYN, respectively (n = 25 images obtained from n = 2 independent experiments were used for each protein).

utero electroporation (IUE) at E15.5 and analyzed the development of newly generated cortical pyramidal neurons (PNs) derived from shRNA#2-positive progenitors at P7. Whereas the knockdown (KD) of KIAA1107 did not affect radial migration of neural progenitors to layer II/III of the somatosensory cortex (Figures 4D and 4E), it significantly impaired maturation of PNs that exhibited an aberrant morphology with a significant reduction of total number and length of neurites (Figures 4F and 4G).

These data suggest a crucial role of KIAA1107 in the early stages of *in vitro* and *in vivo* neuronal development, when active SV exo/endocytotic activity at the growth cone is essential for

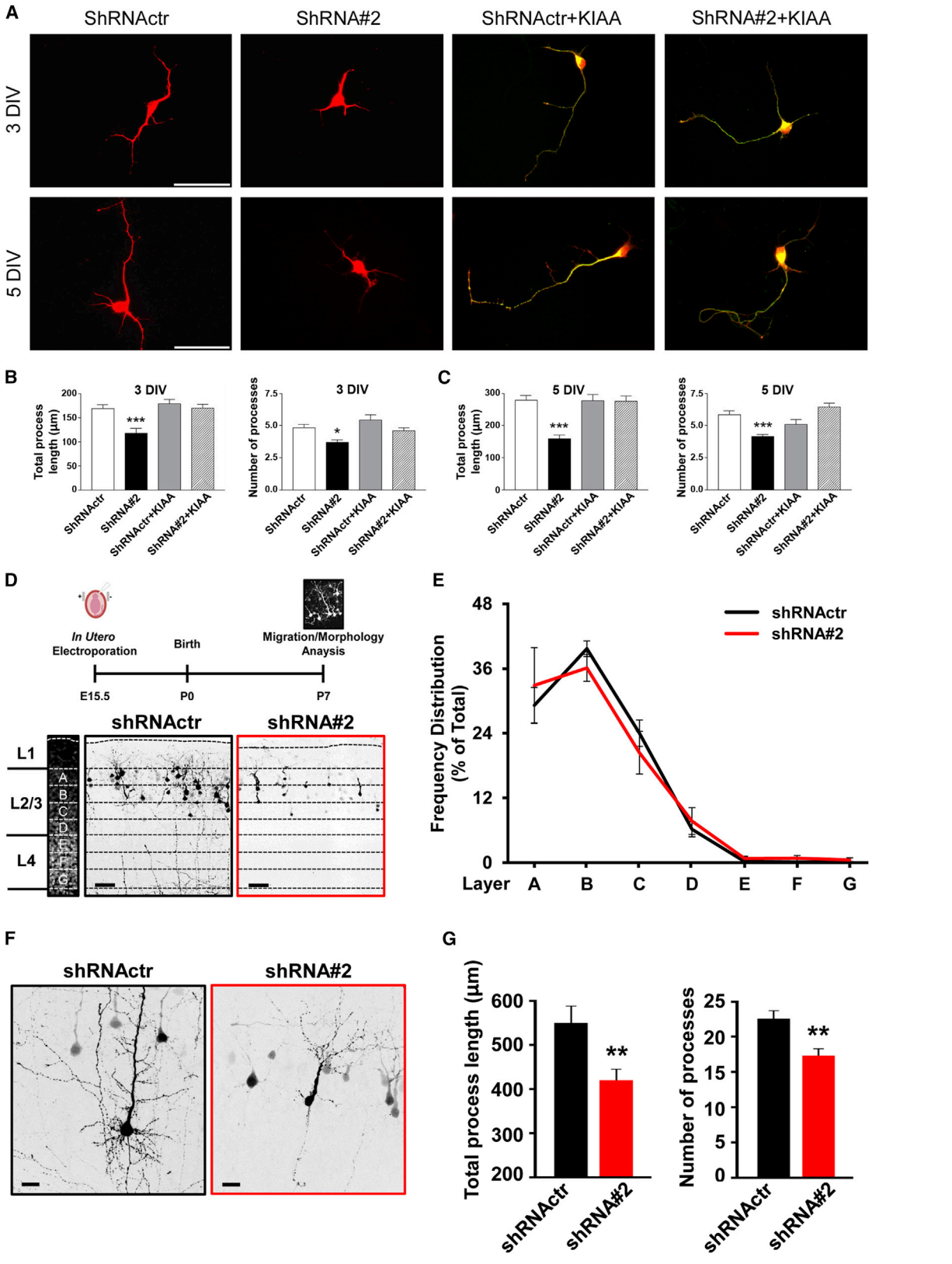

(legend on next page)

process outgrowth (Matteoli et al., 1992; Sabo and McAllister, 2003).

KIAA1107 Markedly Alters the Synaptic Ultrastructure

In view of the potential implication of KIAA1107 in SV endocytosis at mature synapses, we examined the presynaptic ultrastructure of KIAA1107-KD neurons by performing conventional transmission electron microscopy (TEM). Mouse cortical neurons were transduced with a lentiviral vector driving the expression of shRNA#2 or shRNActr at 12 DIV. After 5 days, KIAA1107 became undetectable (Figure S5A), whereas no difference in viability was observed between uninfected (ctr) and infected cells (Figure S5B). Notably, KIAA1107-KD synapses were characterized by a markedly reduced density of total SVs (~50% reduction; Figures 5A and 5B), whereas synaptic area, active zone (AZ) length, density of docked SVs, and distribution of SVs with respect to the AZ were comparable to control synapses (Figure 5C). These data were corroborated by a reduced expression level of synaptophysin and AP2 in KIAA1107-KD neurons compared to control (~40% reduction; Figure S5A). Moreover, the density of CCVs was dramatically reduced in silenced synapses (Figure 5B). Finally, KIAA1107-KD synapses displayed enlarged endosome-like structures (~50% increase in size) but with a preserved endosome density (Figure 5B), as confirmed by the increased immunoreactivity of the endosomal marker Rab5 at KIAA1107-KD synapses (Figures S6A and S6B).

To analyze in greater detail the morphology of synaptic terminals, we performed serial sectioning followed by 3D reconstruction of control and KIAA1107-KD synapses (Figure 5D). The morphometric analysis confirmed the severe reduction in the number of SVs and the parallel depletion of CCVs in silenced synapses compared to control (Figure 5E) and revealed that the enlarged endosome-like structures were fully separated from the plasma membrane (Figure 5D). Notably, the ultrastructural effects of KIAA1107 KD were reversible; the silencing phenotype was completely rescued by coinfection of the neurons with EGFP-KIAA1107 (Figures 5D and 5E) resistant to shRNA#2 silencing (Figure S5C). These results show that KIAA1107-silenced synapses, in spite of a normal gross morphology, display severe ultrastructural defects that are consistent with an important role of KIAA1107 in the regulation of SV recycling and in the maintenance of SV pools.

Clathrin/AP2-Mediated Endocytosis Is Impaired in KIAA1107-Silenced Synapses

Mutations in the genes that encode AP2 and other adaptor-like proteins, which are intrinsic components of the clathrin coat and are implicated in the early steps of SV recovery, lead to ultrastructural phenotypes that are similar to that induced by KIAA1107 silencing (González-Gaitán and Jäckle, 1997; Fergestad et al., 1999; Zhang et al., 1998).

To uncover whether SV recycling is impaired in KIAA1107-KD synapses, we imaged shRNActr- and shRNA#2-infected neurons by electron microscopy upon action potential (AP) firing in the presence of soluble horseradish peroxidase (HRP) to visualize the formation of endocytic intermediates.

We first analyzed synapses under conditions of low-frequency stimulation, when compensatory during-stimulus membrane retrieval largely (but not exclusively) occurs through CME (Granseth et al., 2006; Dittman and Ryan, 2009; Kononenko et al., 2014). Samples were fixed under basal conditions, immediately at the end of the field stimulation (200 APs at 5 Hz) or after 2- and 20-min wash in the absence of HRP. At the end of the stimulus, a significantly decreased density of HRP-positive (HRP^+) SVs, HRP^+ CCVs, and HRP^+ endosome-like structures, all representative of active cycling during stimulation, was observed in KIAA1107-KD terminals compared to control (Figures 6A and 6B). Moreover, the percentage of synapses displaying HRP^+ CCVs at the end of the stimulus versus total synapses was decreased by about 75% in silenced neurons compared to control (40.9% ± 2.7% and 10.3% ± 6.9% for shRNActr and shRNA#-2-infected neurons, respectively). After 2-min wash in the absence of HRP, a significant impairment in the formation of HRP^+ SVs was still evident in KIAA1107-KD terminals, whereas the formation of HRP^+ endosomal vacuoles recovered to control levels. Finally, after 20-min wash in the absence of HRP, SVs and endosomal structures lost their HRP content in both experimental groups, indicating an active and complete recovery. These results indicate that, in KIAA1107-KD synapses, the recovery of SVs, budding either directly from the plasma membrane or from endosome-like structures, was delayed during mild stimulation. The formation of HRP^+ endosomal structures derived from either homotypic fusion of CME-derived vesicles or fusion of such vesicles with early endosomes (Heuser and Reese, 1973; Rizzoli et al., 2006; Hoopmann et al., 2010) was

Figure 4. KIAA1107-Silenced Cortical Neurons Display an Impaired Maturation at Early Stages of *In Vitro* and *In Vivo* Development

(A) Representative merged images of 3 and 5 DIV cortical neurons nucleofected before plating with either ShRNActr or ShRNA#2 (red) and Sh-resistant EGFP-KIAA1107 (green). The scale bars represent 50 μm.

(B and C) Quantification of total process length and number of processes at 3 (B) and 5 (C) DIV using ImageJ. Data are means ± SEM (n = 101 and 83 for ShRNActr neurons; n = 98 and 105 for ShRNA#2 neurons; n = 74 and 89 for ShRNActr+KIAA1107 neurons; n = 66 and 61 for ShRNA#2+KIAA1107 neurons; at 3 and 5 DIV, respectively, from n = 3 independent experiments). *$p < 0.05$; ***$p < 0.001$ versus ShRNActr neurons; one-way ANOVA/Bonferroni's multiple comparison test.

(D–G) KIAA1107-silencing *in vivo* does not impair radial migration but causes impairment in pyramidal neurons' morphology.

(D, top) Cartoon depicting the experimental design of the *in vivo* experiments is shown. (Bottom) Representative images of GFP fluorescence in neurons transfected with either ShRNActr (black) or ShRNA#2 (red) in the somatosensory cortex are shown. The slices were counterstained with DAPI to allow the visualization of cortical layers 2/3/4 (L2/3 and L4), here divided in 8 sub-layers (named from A to G, left). The scale bars represent 50 μm.

(E) Quantification of the percentage of total transfected cells in each layer is shown. Data are means ± SEM (n = 8 animals per condition, 1 slice per animal).

(F) Representative high-magnification images of GFP fluorescence in neurons transfected with either ShRNActr (black) or ShRNA#2 (red) in layer II/III of the somatosensory cortex are shown. The scale bars represent 15 μm.

(G) Quantification of total process length (left) and number (right) using ImageJ is shown. Data are means ± SEM (n = 21 cells from 8 different animals for ShRNActr; n = 23 cells from 8 different animals for ShRNA#2); **$p < 0.01$; unpaired Student's t test.

See also Figure S4.

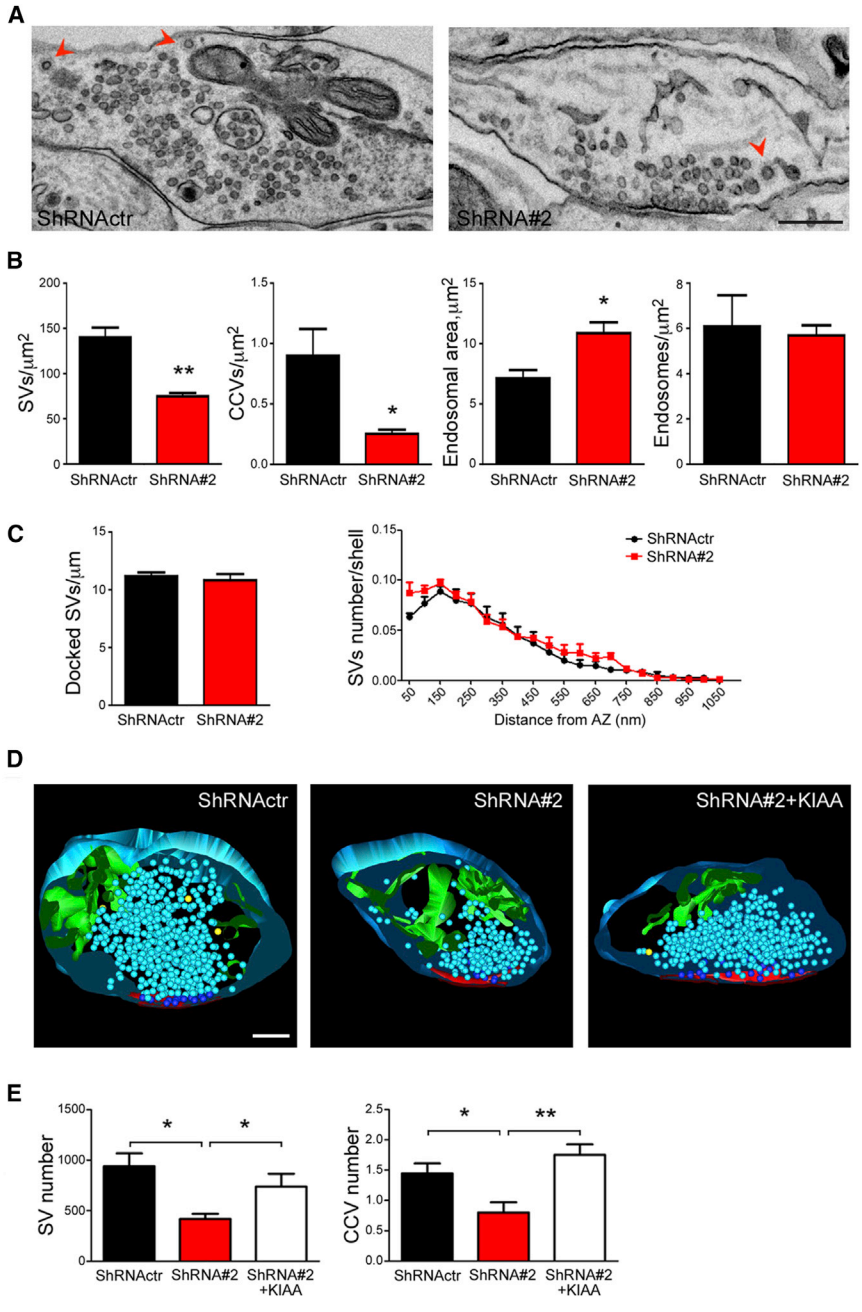

Figure 5. Reduced SV Density and Increased Size of Endosome-like Structures at KIAA1107-Silenced Cortical Synapses

(A) Representative TEM images of nerve terminals from cultured cortical neurons transduced with either ShRNActr or ShRNA#2 at 12 DIV and processed at 17 DIV. Note the reduced SV density in the KIAA1107-KD synapse compared to control (CCVs, red arrowheads). The scale bar represents 200 nm.

(B) Morphometric analysis from serial ultrathin sections obtained from ShRNActr- (black bars) and ShRNA#2- (red bars) treated synapses revealed (from left to right) a reduction in the density of total SVs and CCVs and an increase in the area of endosome-like structures in KIAA1107-KD synapses compared to control. *p < 0.05; **p < 0.01; unpaired Student's t test.

(C) No changes were observed in the density of AZ-docked SVs and in the spatial distribution of SVs in the nerve terminals of KIAA1107-KD neurons compared to control. The density of SVs located within successive 50-nm shells from the AZ was normalized for the total SV content of each terminals and is given as a function of the distance from the AZ. Nerve terminal areas (0.716 ± 0.059 μm^2 and 0.800 ± 0.024 μm^2 for ShRNActr and ShRNA#2-infected neurons, respectively) and AZ lengths (0.350 ± 0.016 μm and 0.335 ± 0.007 μm for ShRNActr and ShRNA#2-infected neurons, respectively) were similar in the two experimental groups. Data are means ± SEM (n = 157 and n = 160 synapses for ShRNActr and ShRNA#2-infected neurons, respectively, from n = 4 independent preparations).

(D) Representative 3D reconstructions of synaptic terminals from 60-nm-thick serial sections obtained from cortical neurons confirmed the severe reduction in SV (light blue spheres) and CCV (yellow spheres) number in ShRNA#2-treated neurons, which was completely rescued in ShRNA#2+KIAA1107-treated neurons. Endosomal structures (green), not connected with the plasma membrane, are also visible. The AZ and AZ-docked SVs are shown in red and blue, respectively. The scale bar represents 200 nm.

(E) Morphometric analysis of the number of SVs and CCVs in 3D-reconstructed synapses from neurons transduced with ShRNActr (black bars), ShRNA#2 (red bars), or ShRNA#2+KIAA1107 (white bars). Docked SVs (19.3 ± 2.38, 14.57 ± 2.37, and 20.37 ± 4.15 for ShRNActr, ShRNA#2, and ShRNA#2+KIAA1107-infected neurons, respectively) were similar in the three experimental groups. Data are means ± SEM (n = 10 synapses per genotype from n = 3 independent preparations). *p < 0.05; **p < 0.01; one-way ANOVA/Bonferroni's multiple comparison test.

See also Figures S5 and S6.

also delayed in silenced terminals compared to controls. The increased endosomal size observed in silenced synapses both under basal conditions (Figures 5B, S6A, and S6B) and after stimulation (Figure S6C) is compatible with a longer retention of SVs at endosomal level, strongly suggesting an impaired clathrin-mediated SV reformation from endosomal structures.

When neurons were stimulated at higher frequency (200 APs at 40 Hz), i.e., a frequency known to trigger fast membrane retrieval via endocytic intermediates upstream of clathrin-coat assembly (Clayton et al., 2008; Cheung et al., 2010; Kononenko et al., 2014; Watanabe et al., 2013, 2014), a decreased density of HRP^+ SVs was observed only at the end of the stimulus in KIAA1107-KD terminals compared to control (Figure 6C), evidence of a moderate impairment of SV reformation at this intense activity level. HRP^+ CCVs were nearly absent in both genotypes, consistent with the idea that CME is largely dispensable for

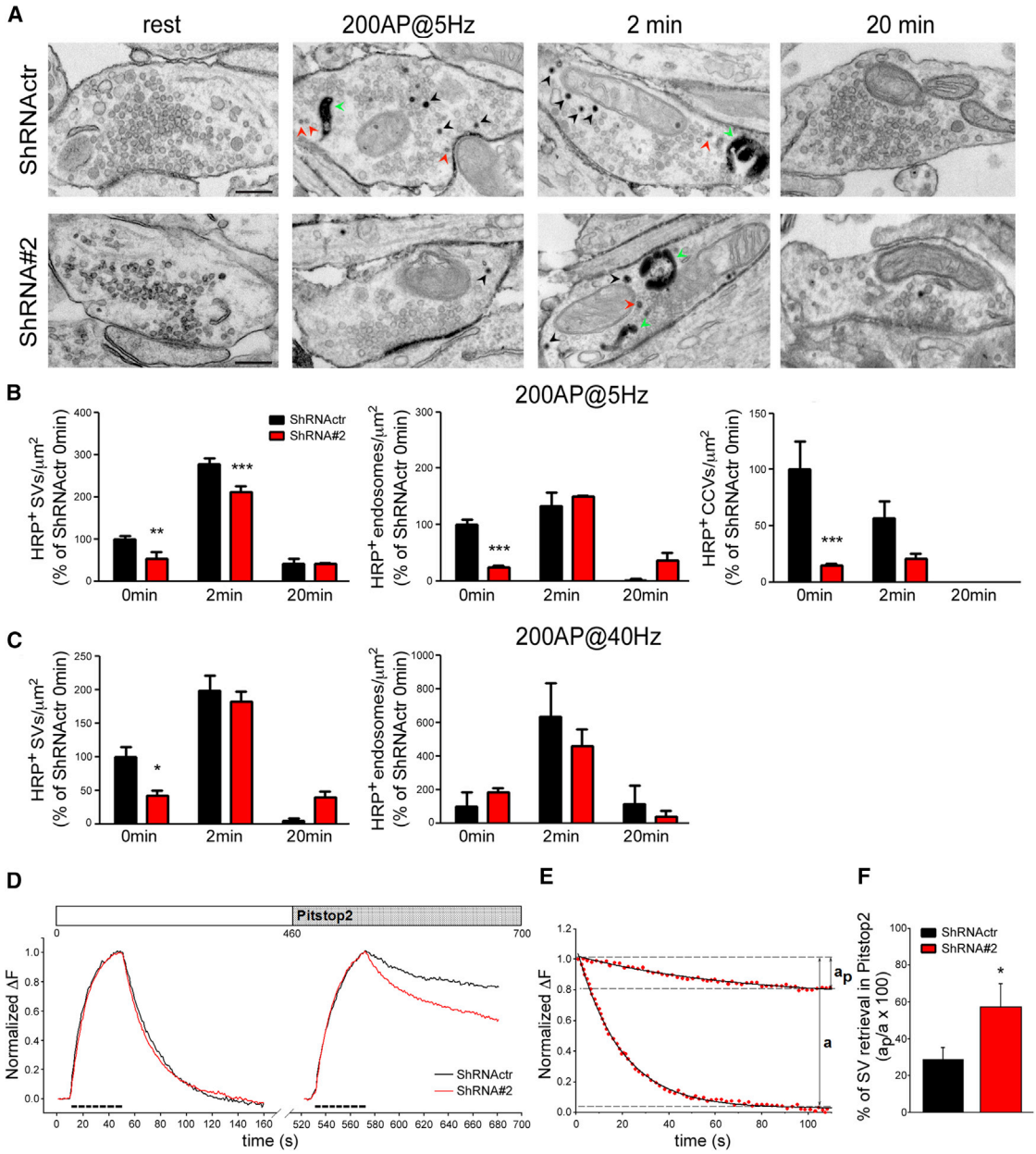

Figure 6. KIAA1107 Knockdown Impairs Clathrin-Mediated Endocytosis in Cortical Synapses

(A) Representative TEM images of presynaptic terminals from control (ShRNActr) and KIAA1107-KD (ShRNA#2) neurons infected at 12 DIV and stimulated at 17 DIV with 200 APs at 5 Hz in the presence of soluble HRP. Synaptic ultrastructure was evaluated by fixing neurons under basal conditions (rest), immediately after the stimulus (0 min), and after 2 or 20 min of recovery in the absence of HRP (HRP$^+$ SVs, black arrowheads; HRP$^+$ CCVs, red arrowheads; HRP$^+$ endosomes, green arrowheads). The scale bars represent 200 nm.

(B and C) Morphometric analysis of HRP-labeled structures after the train stimulation at 5 (B) and 40 (C) Hz (200 APs). The density of HRP-positive (HRP$^+$) SVs, HRP$^+$ endosome-like structures, and HRP$^+$ CCVs in control (black bars) and KIAA1107-KD (red bars) neurons are reported as mean (±SEM) percentages of the respective values observed in the control (ShRNActr) group at 0 min (5 Hz: ShRNActr HRP$^+$SVs, 3.15 ± 0.25; ShRNActr HRP$^+$CCVs, 0.90 ± 0.23; ShRNActr HRP$^+$endosomes, 1.11 ± 0.17; 40 Hz: ShRNActr HRP$^+$SVs, 1.54 ± 0.23; ShRNActr HRP$^+$endosomes, 0.1 ± 0.07). n = 150 and n = 120 images per genotype for the 5- and 40-Hz protocols, respectively, from n = 4 independent preparations. *p < 0.05; **p < 0.01; ***p < 0.001 across genotype, two-way ANOVA/Bonferroni's multiple comparison test.

(D) Ensemble average normalized traces of SypHy fluorescence plotted for control (black trace, n = 8) and KIAA1107-KD (red trace, n = 5) neurons sequentially stimulated with 200 APs at 5 Hz (dotted line) in the absence or presence of 30 µM Pitstop-2.

(E) Representative control data points (red dots) and relative fitting (black traces) by a single exponential function ($y = y_0+a^{-bx}$). The *a* values in the absence (*a*) or presence (a_p) of Pitstop-2 are shown.

(legend continued on next page)

plasma membrane retrieval at this stimulation frequency (Kononenko et al., 2014; Park et al., 2016). In addition, the density of HRP^+ endosomal vacuoles was not altered in silenced synapses (Figure 6C), although their size was increased also at this stimulation frequency (Figure S6D).

We then used Synaptophysin-pHluorin (SypHy) (Tagliatti et al., 2016), co-expressed in hippocampal neurons transduced with either shRNActr or shRNA#2, to further assay membrane recycling following low-frequency stimulation (200 APs at 5 Hz). Surprisingly, no differences in the fluorescence increase, indicative of the rate of release, as well as in the fluorescence decay, representative of post-stimulus endocytosis, were observed in KIAA1107-KD synapses compared to control synapses (Figure 6D). The inability of the SypHy assay to detect an endocytic phenotype in silenced terminals could in principle be due either to a compensatory SV membrane retrieval contributed by clathrin-independent endocytosis (CIE) or, alternatively, to a major involvement of KIAA1107 in SV budding from endosomes rather than from the presynaptic membrane. To sort this out, we challenged neurons with the clathrin inhibitor Pitstop-2 (von Kleist et al., 2011; Figure 6D). The inhibitory effect of Pitstop-2 on endocytosis was severe in both control and KIAA1107-KD synapses, despite the presence of a modest compensation mediated by CIE in the latter (Figures 6D–6F). This suggests that KIAA1107 silencing does not primarily impair SV membrane retrieval or vesicle reacidification but rather SV reformation from endosomes.

In summary, these functional data provide strong evidence that KIAA1107 plays an important role both in CME at the plasma membrane and in the reformation of SVs by clathrin coats budding from endosomes. The kinetics of SV reformation, especially under conditions of low-frequency activity when CME is the predominant pathway for SV recycling, is affected by KIAA1107 silencing. Based on these data, we named the KIAA1107 protein APache, for AP2-interacting clathrin-endocytosis protein.

APache-Silenced Autaptic Neurons Exhibit Impaired Presynaptic Function

To determine whether APache plays a role in synaptic transmission, we performed whole-cell patch-clamp recordings in autaptic hippocampal neurons silenced for APache at 6 DIV and analyzed 5 or 6 days after infection. We preliminarily analyzed the effects of APache silencing on the autapse density and found that the density of synaptic contacts was preserved in APache-KD autaptic neurons (Figure S7A).

Then, we proceeded to the analysis of synaptic transmission. Neurons were stimulated with paired stimuli (50-ms interpulse interval) to evaluate evoked excitatory postsynaptic current (eEPSC) amplitude and paired-pulse facilitation, a presynaptic form of short-term plasticity and an indirect measure of the release probability (Pr) (Fioravante and Regehr, 2011). APache-KD neurons displayed a significant reduction of eEPSC amplitude in response to single stimuli but no changes in paired-pulse facilitation (Figures 7A and 7B). To investigate which of the quantal parameters of release was responsible for the decreased synaptic strength in APache-KD synapses, the cumulative eEPSC amplitude analysis was performed by subjecting neurons to high-frequency trains (2 s at 40 Hz) that induce a complete depletion of the readily releasable pool of SVs (RRP) (Figures 7C–7E). Under this condition, the depression during the steady-state phase is limited by the constant recycling of SVs so that an equilibrium is reached between released and recycled SVs (Schneggenburger et al., 1999). The analysis showed that the RRP size was significantly decreased in APache-KD neurons, to the same extent of the reduction in eEPSC amplitude, whereas Pr was not affected (Figure 7F). This suggests that the impairment in evoked release in APache-KD neurons is likely to involve the constant replenishment of the RRP by the recycling SV pool. Despite the change in RRP, the dynamics of facilitation and depression during the 2-s train at 40 Hz were not significantly affected in silenced neurons compared to control (Figure 7D). Because the various endocytic mechanisms are known to be recruited in a frequency-dependent manner, autaptic neurons were challenged with short 2-s trains at frequencies ranging from 5 to 20 Hz and with a long 30-s train at 10 Hz to analyze the expression of facilitation/depression over time (Figures 7G, 7H, S7B, and S7C). APache-silenced neurons exhibited a more pronounced depression that was tightly dependent on the stimulus frequency. Synaptic depression was faster, more intense, and prolonged in APache-KD synapses during 5-Hz stimulation (Figures 7G and 7H) and progressively attenuated with the increase in stimulation frequency (Figure S7B). The strong increase in synaptic depression at 5 Hz, consistent with the RRP depletion and inactivation of release sites (Fioravante and Regehr, 2011), is likely due, similarly to other endocytic mutants (Milosevic et al., 2011), to the impaired clathrin-mediated recycling of SVs. APache silencing was also associated with an accelerated kinetics of depression evoked by long trains (30 s at 10 Hz; Figure S7C). In addition, post-tetanic potentiation (PTP), a form of short-term plasticity evoked after a short high-frequency stimulation and contributed by increases in both Pr and RRP (Valente et al., 2012), was also impaired in APache-KD neurons (~35% reduction; Figure S7D), consistent with the SV depletion observed upon APache silencing.

DISCUSSION

In the present study, using the bioinformatics GAMMA program to search for uncharacterized genes associated with SVs and presynaptic physiology, we identified KIAA1107 with the highest score. The mouse KIAA1107 main isoform is a protein of 1,088 aas lacking both structural data and known function. Our results demonstrate that KIAA1107 is an AP2 interactor that plays a role in early neuronal development and in CME at mature

(F) The a_p/a ratio, representing the percentage of retrieved SVs in the presence of Pitstop-2 versus the retrieved SVs in its absence, is plotted for control (black bar, n = 8) and KIAA1107-KD (red bar, n = 5) synapses. Data are means ± SEM from the indicated number of coverslips from n = 3 independent preparations. *$p < 0.05$; unpaired Student's t test.
See also Figure S6.

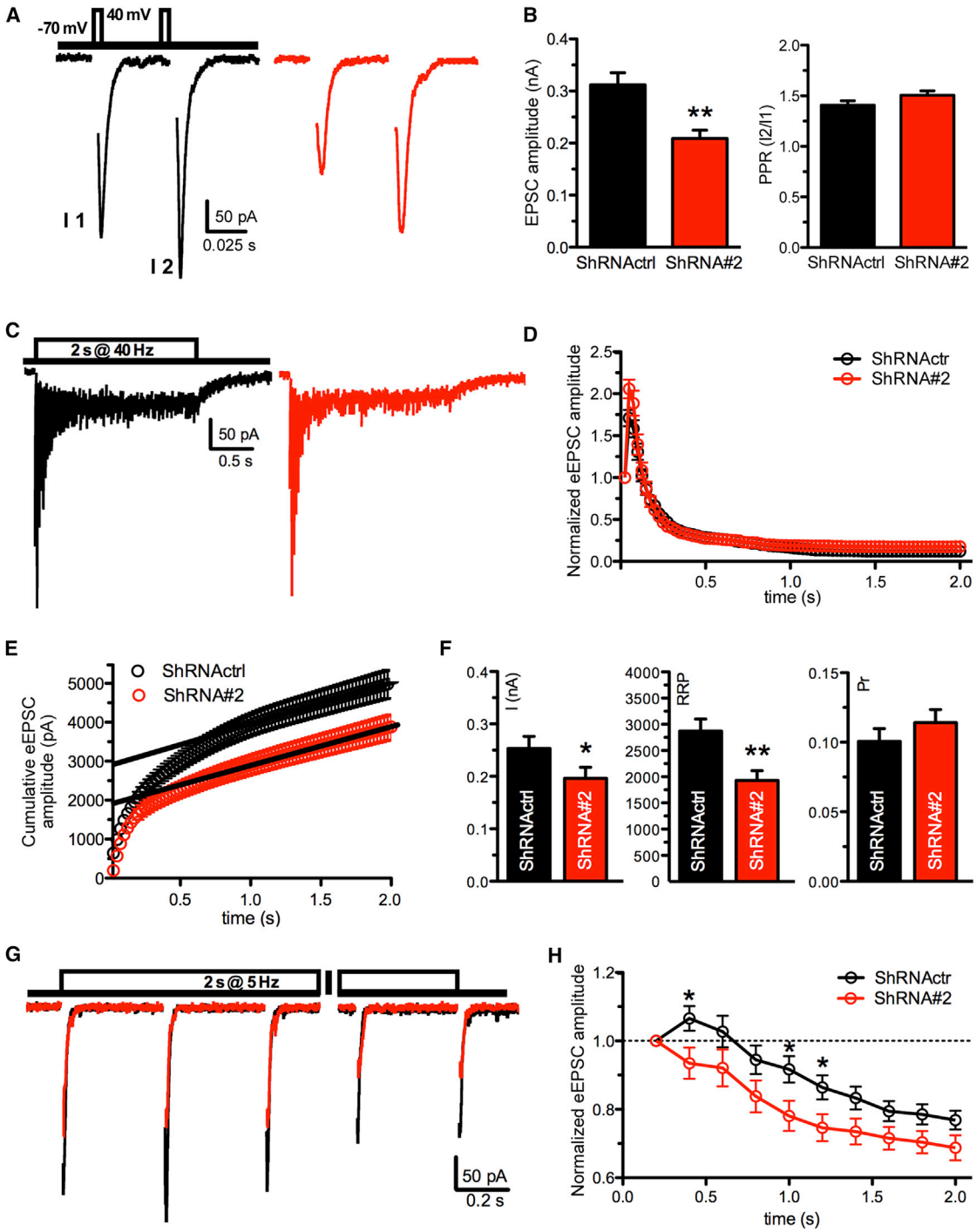

Figure 7. KIAA1107 Silencing Decreases Evoked Excitatory Synaptic Transmission and Enhances Synaptic Depression in Autaptic Hippocampal Neurons

(A) Representative eEPSCs recorded in autaptic neurons transduced with either ShRNActr (black traces, n = 67) or ShRNA#2 (red traces, n = 63). eEPSCs were elicited by clamping the cell at −70 mV and stimulating it with two voltage steps to + 40 mV lasting 0.5 ms at an inter-stimulus interval of 50 ms (inset).

(B) eEPSC amplitude evoked by the first pulse (I1, left) and paired-pulse ratio (PPR) (I2/I1, right) recorded under the same conditions of (A).

(C) Representative recordings of eEPSC evoked by a 2-s tetanic stimulation at 40 Hz in autaptic neurons transduced with ShRNActr (black) or ShRNA#2 (red).

(D) Normalized values of eEPSC amplitude showing the time course of synaptic facilitation and depression in autaptic neurons stimulated as in (C).

(E) Cumulative mean amplitude profiles for eEPSCs during the tetanic stimulation shown in (C) in neurons infected with ShRNActr (black trace, n = 40) or ShRNA#2 (red trace, n = 37). Data points in the 1- to 2-s range were fitted by linear regression and backextrapolated to time 0 (solid lines) to estimate the RRP.

(legend continued on next page)

synapses. We named the protein APache and consider it a molecular component of the clathrin/AP2-dependent endocytic machinery that regulates the fate of endocytosed SVs.

CME has a range of different functions that also include sampling the cell environment for growth and guidance cues and bringing nutrients into cells in developing neurons. An active SV exo/endocytosis in the growth cone has been demonstrated in cultured neurons (Matteoli et al., 1992; Sabo and McAllister, 2003). The present data suggest that, in developing neurons, APache may function in vesicle trafficking events. APache is expressed since the early stages of neuronal development and is present in axonal processes and growth cones, where it promotes neuronal maturation and process outgrowth both *in vitro* and *in vivo*. Moreover, the expression level of AP2 is reduced in developing silenced neurons. It is tempting to speculate that the developmental role of APache is obtained through the clathrin-mediated trafficking pathways that control axon and dendrite outgrowth in developing neurons that are characterized by abundant CCVs (Roos and Kelly, 1999). Intriguingly, AP180 and CALM, two clathrin assembly proteins involved in CME, also play critical roles in controlling the outgrowth of axons and dendrites in embryonic hippocampal neurons (Bushlin et al., 2008), and their silencing elicits morphological phenotypes reminiscent of those of APache-depleted cortical neurons.

Other potential interactors detected in the MS scans can contribute to the effects of APache in neuronal development. NUMBL, an endocytic adaptor binding to the AP2 complex and Eps15 and implicated in CME and neurite outgrowth (Santolini et al., 2000; Sestan et al., 1999; Nishimura et al., 2003) was identified as an APache interactor in our study as well as in a recent proteomic study (Hein et al., 2015). Dynactin, a direct AP2-binding partner that regulates bidirectional transport of vesicles in mammalian neurons, microtubule advance during growth cone remodeling (Kwinter et al., 2009; Grabham et al., 2007), and trafficking of BDNF-TrkB signaling endosomes (Kononenko et al., 2017; Zhou et al., 2012) was also identified as an APache interactor. Thus, in addition to its role in endocytosis at the plasma membrane, APache may also play a role in the internal vesicular/endosomal transport.

Several lines of evidence suggest a potential role for APache in CME at mature synapses. APache is most abundant in brain and, in mature synapses, is concentrated at presynaptic terminals, where it colocalizes with synaptotagmin-1, AP2, and dynamin-1. We have identified AP2 as an APache interactor with the following evidence: (1) APache co-immunoprecipitates with AP2α and β subunits from brain extracts, suggesting that it may participate in the complex network of interactions regulating CME and SV recycling; (2) APache is enriched in CCVs to levels comparable to the coat proteins AP2 and clathrin and at a much larger extent than CME accessory proteins, such as dynamin, synaptojanin, amphiphysin, or endophilin; and (3) APache can be stripped from purified CCVs by treatment with Tris buffer, a well-established procedure to remove coat components from SVs. Synapses that lack APache display the typical features of endocytic mutants. The ultrastructural changes include a severe depletion of SVs and CCVs and the presence of enlarged endosome-like structures. The morpho-functional phenotype of APache silencing consists in a global impairment of SV recycling and synaptic strength that peaks under conditions of low-frequency activity.

Mature synapses use multiple activity-dependent SV recycling mechanisms that operate in parallel and influence neurotransmitter release and synaptic plasticity: "kiss and run"; CME; and clathrin-independent mechanisms (i.e., ultrafast or bulk endocytosis). Whereas the retrieval of the majority of fully fused SVs during mild electrical activity occurs through CME, with vesicles reforming directly from the plasma membrane or from endosomal structures (Hoopmann et al., 2010; Uytterhoeven et al., 2011), during intense high-frequency activity, SV membranes are mostly retrieved through CIE.

The experimental evidence indicates that APache is required to maintain normal SV recycling and RRP refilling at the synapse under conditions of mild stimulation by acting in the clathrin/AP2-mediated regeneration of SVs both from the cell surface and from internalized endosomal structures. The latter mechanism seems to be the predominant one, given the lack of effect of APache silencing on SV reacidification in the SypHy assay. Consistent with this, enlarged endosomal vacuoles accumulate at silenced synapses and may contribute to the depression of neurotransmitter release. On the other hand, APache is dispensable for plasma membrane retrieval at high frequencies, although it may be required for the clathrin-mediated SV reformation from endosomal vacuoles generated by CIE. This model is consistent with prior data demonstrating that silencing or conditional knockout of either AP2 (Kim and Ryan, 2009; Kononenko et al., 2014) or AP2-associated endocytic adaptor proteins (Fergestad et al., 1999; Kononenko et al., 2013) significantly slows down, but does not abolish, SV endocytosis and validates the view that alternative molecules or different mechanisms that normally operate in conjunction with AP2 are required to ensure efficient SV and cargo retrieval over a wide range of stimulation frequencies.

Although further structure function studies will be needed to unravel the precise molecular mechanisms that mediate the described APache functions, the identification of an additional molecular component of the complex endocytic pathway is a

(F) Quantal analysis of release in neurons infected with ShRNActr (black bars) or ShRNA#2 (red bars). From left to right, amplitude of the first eEPSC, RRP size, and probability of release (Pr) are shown.

(G) Representative recordings of eEPSC evoked by a 2-s tetanic stimulation at 5 Hz in autaptic neurons transduced with either ShRNActr (black, n = 31) or ShRNA#2 (red, n = 21).

(H) Normalized values of eEPSC amplitude showing the time course of synaptic facilitation and depression in autaptic neurons stimulated as in (G). In all graphed currents, stimulation artifacts were blanked for clarity. Data are means ± SEM from the indicated numbers of cells recorded at least from n = 3 independent cell culture preparations. *$p < 0.05$; **$p < 0.01$; unpaired Student's t test or Mann-Whitney U test.

See also Figure S7.

step forward for getting insights into fundamental aspects of SV recycling in the healthy and diseased brain.

EXPERIMENTAL PROCEDURES

C57BL/6J mice and Sprague-Dawley rats of either sex were from Charles River Laboratories (Calco, Italy). All experiments, conducted at various stages of development (from E18 to adult mice), were carried out in accordance with the guidelines established by the European Communities Council (directive 2010/63/EU of March 4, 2014) and were approved by the Italian Ministry of Health. The standard procedures for western blotting, CCV purification, pull-down and co-immunoprecipitation assays, immunocytochemistry, real-time PCR, and cultures of low-density and autaptic neurons are reported in detail in the Supplemental Experimental Procedures.

GAMMA

GAMMA relies on identifying gene-gene expression correlations using thousands of publicly available microarray datasets available from the GEO repository. Additional data are reported in the Supplemental Experimental Procedures.

KIAA1107 Antibodies and Constructs

A polyclonal KIAA1107-specific antibody was raised in the rabbit against a conserved region comprising aas 732–894 of mouse KIAA1107. cDNA of *Kiaa1107* was amplified from total mRNA extracted from mouse brain and inserted into the p3XFLAG-CMV-14 or p277.pCCLsin.cPPT.hPGK.eGFP.WPRE vector. shRNAs#1–3 and control shRNA were inserted into the pLKO.1-CMV-mCherry lentiviral vector and used to knockdown the endogenous KIAA1107 in neurons. For detailed description of antibodies, constructs, and neuronal and cellular transfection, see the Supplemental Experimental Procedures.

MS Analysis

Sample preparation, LC-MS/MS analysis, database searching, and criteria for protein identification were conducted as reported in details in the Supplemental Experimental Procedures.

IUE

Standard IUE was performed as previously described (Szczurkowska et al., 2016). The images were acquired using a confocal laser-scanning microscope (TCS SP5; Leica Microsystem) or an epifluorescence microscope equipped with Neurolucida (MicroBrightField) software. For detailed procedures and reagents, see the Supplemental Experimental Procedures.

TEM

Low-density cultures of cortical neurons were infected at 12 DIV with either control shRNA or KIAA1107 shRNA and processed for TEM. For detailed procedures, see the Supplemental Experimental Procedures.

Live Imaging and Patch-Clamp Experiments

Optical recordings with Syphy fluorescent probe were performed at 17 DIV (5 days postinfection). Whole-cell patch-clamp recordings were made from autaptic neurons grown on microislands infected at 6 DIV with either control shRNA or KIAA1107 shRNA. For detailed procedures, see the Supplemental Experimental Procedures.

Statistical Analysis

Data with normal distribution were analyzed by one- or two-way ANOVA followed by the Bonferroni's multiple comparison test or the unpaired Student's t test. Non-normally distributed data were analyzed by the Mann-Whitney's U test. Statistical analysis was carried out using Prism (GraphPad Software, La Jolla, CA, USA) and OriginPro-8 (OriginLab, Northampton, MA, USA) software. Significance level was preset to $p < 0.05$. Data were expressed as means ± SEM for number of samples/cells (n) as detailed in the figure legends.

SUPPLEMENTAL INFORMATION

Supplemental Information includes seven figures and one data file and can be found with this article online at https://doi.org/10.1016/j.celrep.2017.11.073.

ACKNOWLEDGMENTS

We thank Dr. Silvia Casagrande (University of Genova, Italy) for assistance in the preparation of primary cultures, Dr. Elena Monzani (San Raffaele Scientific Institute, Milan, Italy) for preparation of lentiviral constructs, and Prof. Luigi Naldini (TIGET, San Raffaele Scientific Institute, Milan, Italy) for the kind supply of the lentiviral vector. This study was supported by research grants from the Italian Ministry of University and Research (FIRB 2010 "Futuro in Ricerca" to S.G.), CARIPLO Foundation (2013 0879 to F.V. and F.B.), and Compagnia di San Paolo (2015.0546 to F.B.). The support of Telethon-Italy (GGP13033 to F.B.) is also acknowledged and NIH grant number 5P20GM103636 (to J.D.W.).

AUTHOR CONTRIBUTIONS

A.P. participated in the design of the experiments and performed research. E.C. performed and analyzed the ultrastructural experiments. F.C.G. and F.C. ran the developmental studies and provided experimental tools. P.V. and G.G. performed the electrophysiological experiments and analyzed the data. D.A. performed the live imaging experiments. M.B. participated in image acquisition. C.M., B.P., and A.S. performed IUE, slice histology, and image acquisition and analysis. A.B. and A.C. performed the MS analysis. A.F. supervised the live imaging experiments. J.D.W. performed the bioinformatic analysis. F.V. contributed to the research design. S.G. performed research, analyzed data, and made the figures. S.G. and F.B. designed and supervised the research and wrote the paper. All authors revised the manuscript.

DECLARATION OF INTERESTS

The authors declare no competing interests.

Received: April 24, 2017
Revised: October 23, 2017
Accepted: November 20, 2017
Published: December 19, 2017

REFERENCES

Bushlin, I., Petralia, R.S., Wu, F., Harel, A., Mughal, M.R., Mattson, M.P., and Yao, P.J. (2008). Clathrin assembly protein AP180 and CALM differentially control axogenesis and dendrite outgrowth in embryonic hippocampal neurons. J. Neurosci. *28*, 10257–10271.

Cheung, G., Jupp, O.J., and Cousin, M.A. (2010). Activity-dependent bulk endocytosis and clathrin-dependent endocytosis replenish specific synaptic vesicle pools in central nerve terminals. J. Neurosci. *30*, 8151–8161.

Clayton, E.L., Evans, G.J., and Cousin, M.A. (2008). Bulk synaptic vesicle endocytosis is rapidly triggered during strong stimulation. J. Neurosci. *28*, 6627–6632.

Conner, S.D., and Schmid, S.L. (2003). Regulated portals of entry into the cell. Nature *422*, 37–44.

Cousin, M.A. (2017). Integration of synaptic vesicle cargo retrieval with endocytosis at central nerve terminals. Front. Cell. Neurosci. *11*, 234.

Dittman, J., and Ryan, T.A. (2009). Molecular circuitry of endocytosis at nerve terminals. Annu. Rev. Cell Dev. Biol. *25*, 133–160.

Fergestad, T., Davis, W.S., and Broadie, K. (1999). The stoned proteins regulate synaptic vesicle recycling in the presynaptic terminal. J. Neurosci. *19*, 5847–5860.

Fioravante, D., and Regehr, W.G. (2011). Short-term forms of presynaptic plasticity. Curr. Opin. Neurobiol. *21*, 269–274.

González-Gaitán, M., and Jäckle, H. (1997). Role of Drosophila alpha-adaptin in presynaptic vesicle recycling. Cell *88*, 767–776.

Gorini, G., Ponomareva, O., Shores, K.S., Person, M.D., Harris, R.A., and Mayfield, R.D. (2010). Dynamin-1 co-associates with native mouse brain BKCa channels: proteomics analysis of synaptic protein complexes. FEBS Lett. *584*, 845–851.

Grabham, P.W., Seale, G.E., Bennecib, M., Goldberg, D.J., and Vallee, R.B. (2007). Cytoplasmic dynein and LIS1 are required for microtubule advance during growth cone remodeling and fast axonal outgrowth. J. Neurosci. *27*, 5823–5834.

Granseth, B., Odermatt, B., Royle, S.J., and Lagnado, L. (2006). Clathrin-mediated endocytosis is the dominant mechanism of vesicle retrieval at hippocampal synapses. Neuron *51*, 773–786.

Hein, M.Y., Hubner, N.C., Poser, I., Cox, J., Nagaraj, N., Toyoda, Y., Gak, I.A., Weisswange, I., Mansfeld, J., Buchholz, F., et al. (2015). A human interactome in three quantitative dimensions organized by stoichiometries and abundances. Cell *163*, 712–723.

Heuser, J.E., and Reese, T.S. (1973). Evidence for recycling of synaptic vesicle membrane during transmitter release at the frog neuromuscular junction. J. Cell Biol. *57*, 315–344.

Hoopmann, P., Punge, A., Barysch, S.V., Westphal, V., Bückers, J., Opazo, F., Bethani, I., Lauterbach, M.A., Hell, S.W., and Rizzoli, S.O. (2010). Endosomal sorting of readily releasable synaptic vesicles. Proc. Natl. Acad. Sci. USA *107*, 19055–19060.

Kasof, G.M., Goyal, L., and White, E. (1999). Btf, a novel death-promoting transcriptional repressor that interacts with Bcl-2-related proteins. Mol. Cell. Biol. *19*, 4390–4404.

Kim, S.H., and Ryan, T.A. (2009). Synaptic vesicle recycling at CNS snapses without AP-2. J. Neurosci. *29*, 3865–3874.

Kononenko, N.L., and Haucke, V. (2015). Molecular mechanisms of presynaptic membrane retrieval and synaptic vesicle reformation. Neuron *85*, 484–496.

Kononenko, N.L., Diril, M.K., Puchkov, D., Kintscher, M., Koo, S.J., Pfuhl, G., Winter, Y., Wienisch, M., Klingauf, J., Breustedt, J., et al. (2013). Compromised fidelity of endocytic synaptic vesicle protein sorting in the absence of stonin 2. Proc. Natl. Acad. Sci. USA *110*, E526–E535.

Kononenko, N.L., Puchkov, D., Classen, G.A., Walter, A.M., Pechstein, A., Sawade, L., Kaempf, N., Trimbuch, T., Lorenz, D., Rosenmund, C., et al. (2014). Clathrin/AP-2 mediate synaptic vesicle reformation from endosome-like vacuoles but are not essential for membrane retrieval at central synapses. Neuron *82*, 981–988.

Kononenko, N.L., Claßen, G.A., Kuijpers, M., Puchkov, D., Maritzen, T., Tempes, A., Malik, A.R., Skalecka, A., Bera, S., Jaworski, J., and Haucke, V. (2017). Retrograde transport of TrkB-containing autophagosomes via the adaptor AP-2 mediates neuronal complexity and prevents neurodegeneration. Nat. Commun. *8*, 14819.

Kwinter, D.M., Lo, K., Mafi, P., and Silverman, M.A. (2009). Dynactin regulates bidirectional transport of dense-core vesicles in the axon and dendrites of cultured hippocampal neurons. Neuroscience *162*, 1001–1010.

Matteoli, M., Takei, K., Perin, M.S., Südhof, T.C., and De Camilli, P. (1992). Exo-endocytotic recycling of synaptic vesicles in developing processes of cultured hippocampal neurons. J. Cell Biol. *117*, 849–861.

Milosevic, I., Giovedi, S., Lou, X., Raimondi, A., Collesi, C., Shen, H., Paradise, S., O'Toole, E., Ferguson, S., Cremona, O., and De Camilli, P. (2011). Recruitment of endophilin to clathrin-coated pit necks is required for efficient vesicle uncoating after fission. Neuron *72*, 587–601.

Nishimura, T., Fukata, Y., Kato, K., Yamaguchi, T., Matsuura, Y., Kamiguchi, H., and Kaibuchi, K. (2003). CRMP-2 regulates polarized Numb-mediated endocytosis for axon growth. Nat. Cell Biol. *5*, 819–826.

Park, J., Cho, O.Y., Kim, J.A., and Chang, S. (2016). Endosome-mediated endocytic mechanism replenishes the majority of synaptic vesicles at mature CNS synapses in an activity-dependent manner. Sci. Rep. *6*, 31807.

Raman, D., Sai, J., Hawkins, O., and Richmond, A. (2014). Adaptor protein2 (AP2) orchestrates CXCR2-mediated cell migration. Traffic *15*, 451–469.

Rizzoli, S.O., Bethani, I., Zwilling, D., Wenzel, D., Siddiqui, T.J., Brandhorst, D., and Jahn, R. (2006). Evidence for early endosome-like fusion of recently endocytosed synaptic vesicles. Traffic *7*, 1163–1176.

Robinson, M.S. (2004). Adaptable adaptors for coated vesicles. Trends Cell Biol. *14*, 167–174.

Roos, J., and Kelly, R.B. (1999). The endocytic machinery in nerve terminals surrounds sites of exocytosis. Curr. Biol. *9*, 1411–1414.

Sabo, S.L., and McAllister, A.K. (2003). Mobility and cycling of synaptic protein-containing vesicles in axonal growth cone filopodia. Nat. Neurosci. *6*, 1264–1269.

Saheki, Y., and De Camilli, P. (2012). Synaptic vesicle endocytosis. Cold Spring Harb. Perspect. Biol. *4*, a005645.

Santolini, E., Puri, C., Salcini, A.E., Gagliani, M.C., Pelicci, P.G., Tacchetti, C., and Di Fiore, P.P. (2000). Numb is an endocytic protein. J. Cell Biol. *151*, 1345–1352.

Schmid, E.M., and McMahon, H.T. (2007). Integrating molecular and network biology to decode endocytosis. Nature *448*, 883–888.

Schneggenburger, R., Meyer, A.C., and Neher, E. (1999). Released fraction and total size of a pool of immediately available transmitter quanta at a calyx synapse. Neuron *23*, 399–409.

Schroer, T.A. (2004). Dynactin. Annu. Rev. Cell Dev. Biol. *20*, 759–779.

Sestan, N., Artavanis-Tsakonas, S., and Rakic, P. (1999). Contact-dependent inhibition of cortical neurite growth mediated by notch signaling. Science *286*, 741–746.

Slepnev, V.I., and De Camilli, P. (2000). Accessory factors in clathrin-dependent synaptic vesicle endocytosis. Nat. Rev. Neurosci. *1*, 161–172.

Soykan, T., Maritzen, T., and Haucke, V. (2016). Modes and mechanisms of synaptic vesicle recycling. Curr. Opin. Neurobiol. *39*, 17–23.

Szczurkowska, J., Cwetsch, A.W., dal Maschio, M., Ghezzi, D., Ratto, G.M., and Cancedda, L. (2016). Targeted in vivo genetic manipulation of the mouse or rat brain by in utero electroporation with a triple-electrode probe. Nat. Protoc. *11*, 399–412.

Tagliatti, E., Fadda, M., Falace, A., Benfenati, F., and Fassio, A. (2016). Arf6 regulates the cycling and the readily releasable pool of synaptic vesicles at hippocampal synapse. eLife *5*, e10116.

Tojima, T., Itofusa, R., and Kamiguchi, H. (2010). Asymmetric clathrin-mediated endocytosis drives repulsive growth cone guidance. Neuron *66*, 370–377.

Traub, L.M., and Bonifacino, J.S. (2013). Cargo recognition in clathrin-mediated endocytosis. Cold Spring Harb. Perspect. Biol. *5*, a016790.

Uytterhoeven, V., Kuenen, S., Kasprowicz, J., Miskiewicz, K., and Verstreken, P. (2011). Loss of skywalker reveals synaptic endosomes as sorting stations for synaptic vesicle proteins. Cell *145*, 117–132.

Valente, P., Casagrande, S., Nieus, T., Verstegen, A.M., Valtorta, F., Benfenati, F., and Baldelli, P. (2012). Site-specific synapsin I phosphorylation participates in the expression of post-tetanic potentiation and its enhancement by BDNF. J. Neurosci. *32*, 5868–5879.

Valtorta, F., Meldolesi, J., and Fesce, R. (2001). Synaptic vesicles: is kissing a matter of competence? Trends Cell Biol. *11*, 324–328.

van Hille, B., Richener, H., Evans, D.B., Green, J.R., and Bilbe, G. (1993). Identification of two subunit A isoforms of the vacuolar H(+)-ATPase in human osteoclastoma. J. Biol. Chem. *268*, 7075–7080.

von Kleist, L., Stahlschmidt, W., Bulut, H., Gromova, K., Puchkov, D., Robertson, M.J., MacGregor, K.A., Tomilin, N., Pechstein, A., Chau, N., et al. (2011). Role of the clathrin terminal domain in regulating coated pit dynamics revealed by small molecule inhibition. Cell *146*, 471–484.

Watanabe, S., Rost, B.R., Camacho-Pérez, M., Davis, M.W., Söhl-Kielczynski, B., Rosenmund, C., and Jorgensen, E.M. (2013). Ultrafast endocytosis at mouse hippocampal synapses. Nature *504*, 242–247.

Watanabe, S., Trimbuch, T., Camacho-Pérez, M., Rost, B.R., Brokowski, B., Söhl-Kielczynski, B., Felies, A., Davis, M.W., Rosenmund, C., and Jorgensen, E.M. (2014). Clathrin regenerates synaptic vesicles from endosomes. Nature *515*, 228–233.

Wren, J.D. (2009). A global meta-analysis of microarray expression data to predict unknown gene functions and estimate the literature-data divide. Bioinformatics *25*, 1694–1701.

Zhang, B., Koh, Y.H., Beckstead, R.B., Budnik, V., Ganetzky, B., and Bellen, H.J. (1998). Synaptic vesicle size and number are regulated by a clathrin adaptor protein required for endocytosis. Neuron *21*, 1465–1475.

Zhou, B., Cai, Q., Xie, Y., and Sheng, Z.-H. (2012). Snapin recruits dynein to BDNF-TrkB signaling endosomes for retrograde axonal transport and is essential for dendrite growth of cortical neurons. Cell Rep. *2*, 42–51.

Cell Reports, Volume *21*

Supplemental Information

APache Is an AP2-Interacting Protein Involved in Synaptic Vesicle Trafficking and Neuronal Development

Alessandra Piccini, Enrico Castroflorio, Pierluigi Valente, Fabrizia C. Guarnieri, Davide Aprile, Caterina Michetti, Mattia Bramini, Giorgia Giansante, Bruno Pinto, Annalisa Savardi, Fabrizia Cesca, Angela Bachi, Angela Cattaneo, Jonathan D. Wren, Anna Fassio, Flavia Valtorta, Fabio Benfenati, and Silvia Giovedì

SUPPLEMENTAL EXPERIMENTAL PROCEDURES:

GlobAl Microarray Meta-Analysis (GAMMA)

GAMMA is a program previously developed to identify highly correlated transcripts within microarray experiments, which can then be used to infer function, phenotype, genetic network and disease relevance for uncharacterized genes (Wren, 2009). The underlying assumption is that genes that co-vary across many different experimental conditions might also share functional and phenotypic similarities, and be involved in similar biological processes. Identification of these predicted commonalities is achieved by a literature-based analysis to search for co-occurrence of the top 40 correlated genes within MEDLINE abstracts with biological "entities", i.e. diseases, chemicals, phenotypes and biological processes as defined by other public databases (e.g., Entrez Gene, OMIM, CHEMID, etc). The approach is well suited to guide experimentation for uncharacterized genes, since an important experimental consideration in genetic disruption studies is to know what cell type a gene is relevant to and what the potential phenotypic consequences of disruption are. It has been previously successful in predicting phenotype and function for several other uncharacterized or poorly characterized genes, which were established via experimental testing (Gandhapudi et al., 2015; Lupu et al., 2011; Daum et al., 2009).

Generation of the anti-KIAA1107 antibody

A polyclonal KIAA1107-specific antibody was raised in the rabbit against a His-Tag fusion protein comprising aa 732-894 of mouse KIAA1107. This peptide was produced in *E. coli* and purified in quantities sufficient for the immunization protocol. Immunization was conducted by following standard procedures, and the antibody was affinity-purified on a CNBr-Sepharose column coupled to the immunogen peptide. (1.15 mg/ml in glycine 0.1 M, NaCl 0.5 M pH 2.5, Tris-HCl 1M pH 8.0, final pH 7.0). The polyclonal anti-KIAA1107 antibody was tested and proved to react with mouse, rat and human and useful for western blotting, immunocytochemistry and immunoprecipitation.

Generation of *Kiaa1107* plasmids and *Kiaa1107* shRNAs

Total RNA was extracted from the cortex of adult mouse brain using the RNeasy Mini kit (QIAGEN, #74104), and synthetic cDNA prepared using the SuperScript® III First-Strand synthesis System (ThermoFisher Scientific, #18080-051). The *Kiaa1107* sequence (from ATG to stop codon) was amplified by PCR by using the QIAGEN® LongRange PCR kit (QIAGEN, #206401) using the following primers, with the addition of restriction sites (underlined) for the subsequent cloning:

mKIAA1107 mKATE fw (SalI): 5' AT<u>GTCGAC</u>ATGCACTTAGATGATCAGC 3'
mKIAA1107 mKATE rv (SacII): 5' AT<u>CCGCGG</u>CTTCTGTACATTACCTGAG 3'
mKIAA1107 FLAG fw (NotI): 5' AT<u>GCGGCC</u>ATGCACTTAGATGATCAGC 3'
mKIAA1107 FLAG rv (EcoRV): 5' AT<u>GATATC</u>AGCTTCTGTACATTACCTGAG 3'

Only one band was amplified in both cases, corresponding to the 3267 bp isoform (NM_001007574). No band corresponding to the 1332 bp isoform (NM_001168557) was amplified. The band was gel-extracted using the QIAquick Gel extraction kit (QIAGEN, #28706), digested with the appropriate restriction enzymes and inserted in frame into the pmKATE2-N vector (Evrogen, #FP182) and p3XFLAG-CMV™-14 Expression Vector (Sigma Aldrich, #E4901), respectively. An EGFP-tagged version of the construct was also generated, starting from the pmKATE2-KIAA1107 vector. Briefly, the KATE2 tag was substituted by EGFP (extracted by PCR from pEGFP-C1, Clontech) through AgeI/SalI digestion. The EGFP-KIAA1107 coding sequence was then inserted into the lentiviral vector p277.pCCLsin.cPPT.hPGK.eGFP.WPRE (gift of Prof. Luigi Naldini, TIGET, San Raffaele Scientific Institute, Milan, Italy) through AgeI and blunted SalI (acceptor) or SacI (donor) digestion.

KIAA1107 fragments (N- and C-terminal) were produced by PCR amplification of the segments of interest from the EGFP-KIAA1107 plasmid with the following primers:

KIAA1107 amino acids 1-600 fw (NotI): 5'- ATT<u>GCGGCCGC</u>AATGCACTTAGATGATCAGCAG -3'
KIAA1107 amino acids 1-600 rv (EcoRV): 5'- ATT<u>GATATC</u>GTACACAGGAAAGCTTTCCCAT -3'
KIAA1107 amino acids 601-1088 fw (NotI): 5'- ATT<u>GCGGCCGC</u>AATGCACTTAGATGATCAGCAG -3'
KIAA1107 amino acids 601-1088 rv (EcoRV): 5'- ATT<u>GATATC</u>GTACACAGGAAAGCTTTCCCAT -3'

Fragments were inserted in p3XFLAG-CMV™-14 Expression Vector (Sigma Aldrich, #E4901), in frame with the FLAG tag.

Based on the sequence of the cloned *Kiaa1107* transcript variant, 3 distinct short hairpin (sh) RNAs were designed (Mission shRNA custom cloning, Sigma-Aldrich):

shRNA#1: CAGCAGGTTCAGGGAATAATT
shRNA#2: GAGCTAGCTATTCATTATTTA
shRNA#3: GTGAGGTAGAATGCATTATTT

ShRNA#1 was designed against the coding sequence, while shRNA#2 and #3 were designed against the 3' untranslated region (UTR). As a negative control, a series of shRNAs with fully unrelated sequence were tested with similar results and the Luciferase shRNA (Sigma-Aldrich) was chosen for the experiments. All shRNAs were purchased as inserted in the bicistronic lentiviral vector pLKO.1-CMVTurboGFP™+shRNA (Sigma-Aldrich). The TurboGFP tag was then replaced by mCherry (from a previously generated pBluescript-mCherry) through SmaI (donor) or blunted NheI

(acceptor) and KpnI digestion. For rescue experiments, the p277-EGFP-KIAA1107 vector was used, being intrinsically resistant to shRNA#2 and #3.
For IUE experiments, shRNAs were cloned in the pRNAT-U6.3Hygro (GenScript) vector. The following oligonucleotides containing shRNAs and protruding ends for BamHI (5') and HindIII (3') restriction sites were synthetized by Sigma-Aldrich:
Sh#2 fw: GATCCCGAGCTAGCTATTCATTATTTACTCGAGTAAATAATGAATAGCTAGCTCTTTTTCCAAA
Sh#2 rv: AGCTTTTGGAAAAAGAGCTAGCTATTCATTATTTACTCGAGTAAATAATGAATAGCTAGCTCGG
Luc fw: GATCCCCGCTGAGTACTTCGAAATGTCCTCGAGGACATTTCGAAGTACTCAGCGTTTTTCCAAA
Luc rv: AGCTTTTGGAAAAACGCTGAGTACTTCGAAATGTCCTCGAGGACATTTCGAAGTACTCAGCGGG
Forward and reverse oligos for each pair were annealed and ligated to cut pRNAT-U6.3Hygro.
All constructs were verified by direct sequencing.

RNA extraction and real time PCR
Total RNA was extracted by using the RNeasy Mini or Micro Kit (Qiagen) and then DNase-treated with the DNA-free DNA Removal kit (Ambion), following manufacturer's instructions. RNA concentration was quantified by using the Nanodrop-1000 spectrophotometer (Thermo Scientific). Retrotranscription was performed on equal amounts of RNA by using the M-MLV Reverse Transcriptase and random primers (Thermo Scientific), following manufacturer's instructions and including RT- negative controls. Real time PCR analyses were performed using the SYBR Green I Master mix (Roche), on a Lightcycler 480 (Roche), with the following protocol: 95 °C for 5 min; 10 s at 95 °C / 20 s at the specific annealing temperature (T_a) / 10 s at 72 °C for 45 cycles; melting curve (heating ramp from 55 °C to 95 °C) in order to check for amplification specificity. The following primers (final concentration 0.25 μM) and annealing temperatures were used: *Kiaa1107* For-1: GGAAGCCTGTGCTCACCAGCTC, *Kiaa1107* Rev-1: GCATGTCCTGATGCTCCCAATCC, Ta=64 °C; *Kiaa1107* For-2: TGAAAGAGAGCCGTCCCACGC, *Kiaa1107* Rev-2: CACTTCCTGCTCACACGCTGC, Ta=64 °C; *H3f3a* For: GTGAAGAAACCTCATCGTTACAGGCCTGGT, *H3f3a* Rev: CTGCAAAGCACCAATAGCTGCACTCTGGAA, Ta=64 °C; *Tbp* For: GAGCTCTGGAATTGTACCGCAG, *Tbp* Rev: CATGATGACTGCAGCAAATCGC, Ta=62 °C; *Hprt* For: CAGACTGAAGAGCTACTGTAATG, *Hprt* Rev: GGGCTGTACTGCTTAACCAGG, Ta=62 °C. Relative quantification of *Kiaa1107* expression was made using the $2^{-\Delta\Delta Ct}$ method (Pfaffl, 2001), normalizing data to the geometric mean of three housekeeping transcripts (*H3f3a, Tbp, Hprt*; Vandesompele et al., 2002) and to a calibrator (liver for tissue expression profile, E18 for cortical tissue samples, 1 DIV for neuronal cultures).

Culture and transfection of primary neurons
Primary cultures of dissociated cortical and hippocampal neurons were prepared from 17/18-day (E17–18) mouse or rat embryos and plated at low density onto poly-D-lysine (0.1 mg/ml, Sigma-Aldrich)-coated 25-mm glass coverslips (6×10^4 cells/coverslip) and 35-mm wells (1×10^6 cells/well). Cells were maintained in a culture medium consisting of Neurobasal (Gibco) supplemented with B-27 (1:50 v/v, Gibco), Glutamax (1% w/v, Gibco), penicillin–streptomycin (1%, Gibco) and kept at 37 °C in a 5% CO_2 humidified atmosphere. Under this culture condition (Neurobasal/B27 medium and low cell density), approximately 85-90% of the cortical neurons are glutamatergic and cultures are almost glia-free (Piccini et al., 2015). Autaptic hippocampal neurons were prepared as previously described (Valente et al., 2016). Briefly, dissociated neurons were plated at very low density (20 cells/mm^2) on microdots (40-300 μm in diameter) obtained by spraying a mixture of poly-D-lysine (0.1 mg/ml) and collagen (0.25 mg/ml) on petri dishes, previously pretreated with 0.15% agarose. For plasmid and ShRNA transfection experiments, neurons (4×10^6) were nucleofected before plating by electroporation with Amaxa basal nucleofector kit for primary neurons (Lonza) with 4 μg of plasmid DNA according to manufacturer's protocol. For lentiviral infection experiments, low-density or autaptic hippocampal neurons were transduced with 5 MOI (multiplicity of infection) of lentiviral vectors into cell medium at 12 or 6 DIV, respectively. After 24 h, the medium was removed and replaced with equal volumes of fresh and conditioned medium (1:1). For rescue experiments, neurons were co-transduced with 5 + 5 MOI of lentiviral vectors. All experiments were performed 5-6 days post-infection.

Culture and transfection of cell lines
COS-7 and SH-SY5Y neuroblastoma cells were cultured in Dulbecco's MEM (DMEM; Gibco) supplemented with 10% fetal calf serum (Gibco), 1% L-glutamine, 100 U/ml penicillin, and 100 μg/ml streptomycin (Gibco) and maintained at 37 °C in a 5% CO_2 humidified atmosphere. For transfection experiments Lipofectamin2000 (Thermo Scientific) was used according to the manufacturer's protocol, and cells were incubated under standard growth conditions for 48 h and then processed.

Immunocytochemistry
Primary cortical neurons (3, 5 or 17 DIV) or autaptic hippocampal neurons (11 DIV) were fixed with 4% paraformaldehyde (Sigma-Aldrich) and 4% sucrose in phosphate-buffered saline (PBS), pH 7.4 for 20 min at room temperature. After several washes in PBS, cells were permeabilized with 0.1% Triton X-100 in PBS for 5 min and blocked with 0.1% Triton X-100, 3% fetal bovine serum in PBS for 30 min. Samples were incubated with the following primary antibodies diluted in blocking solution for 2 h at room temperature: mouse pan-axonal neurofilament marker

(SMI312, 1:500, Covance), rabbit anti-KIAA1107 (1:500, PRIMM), mouse anti-synaptotagmin-1 (1:500, Synaptic Systems), mouse anti-AP2α (1:500, ThermoFisher), mouse anti-dynamin1 (1:500, BD Transduction Laboratories), mouse anti-VAMP2 (1:500, Synaptic Systems), rabbit anti-Rab5 (1:300, Abcam) and rabbit anti-VGLUT1 (1:500, Synaptic Systems). Immunostaining was detected using Alexa 488 or 594-conjugated secondary antibodies (1:500, Thermo Scientific) diluted in blocking solution for 1 h at room temperature. After several washes in PBS, coverslips were mounted using Prolong Gold antifade reagent (Thermo Scientific) containing DAPI (4′, 6′-diamidino-2-phenylindole) for nuclear staining. Images were acquired with an Olympus IX-81 microscope with an MT20 Arc/Xe lamp and a 40X objective, using the Excellence RT software (Olympus, Hamburg, Germany), and analyzed with ImageJ software, NeuronJ plugin, for morphometric analysis based on mCherry fluorescence. Confocal images were acquired with a confocal laser-scanning microscope (SP8, Leica Microsystems GmbH, Wetzlar, Germany) at 40X (1.4 NA) magnification. Offline analysis was performed using the ImageJ software. The Pearson's correlation coefficient was determined according to Adler and Parmryd (2010) from non-processed raw dual channel images using the JACoP plugin of ImageJ. This coefficient has a range of +1 (perfect correlation) to −1 (perfect but negative correlation) with 0 (zero) denoting the absence of a relationship.

Biochemical Procedures

Western blotting and antibodies. Total cell lysates were obtained from COS-7 cells or cortical neuronal cultures at various DIV (from 1 to 21). Cells were lysed in lysis buffer (150 mM NaCl, 50 mM Tris-HCl pH 7.4, 1 mM EDTA, 1% Triton X-100) supplemented with 1 mM PMSF/1 mM pepstatin (Sigma-Aldrich). After 10 min of incubation on ice, lysates were collected and clarified by centrifugation (10 min at 10,000 x g at 4 °C). Brain regions from adult mice or cerebral cortex at various stages of development (from E18 to P60) were homogenized in ice-cold buffered sucrose solution (0.32 M sucrose, 5 mM HEPES, pH 7.4) plus 100 mM NaCl, 1 mM PMSF/1 mM pepstatin, and centrifuged at 1,000 x g for 10 min at 4 °C to obtain a post-nuclear supernatant fraction. Protein concentration was determined using either Bradford (Bio-Rad) or BCA (Thermo Scientific) assay and equivalent amounts of protein were subjected to SDS-PAGE on 10% polyacrylamide gels and blotted onto nitrocellulose membranes (Whatman). Blotted membranes were blocked for 1 h in 5% milk in Tris-buffered saline (10 mM Tris, 150 mM NaCl, pH 8.0) plus 0.1% Triton X-100 and incubated overnight at 4 °C with the following primary antibodies: rabbit anti-βIII-tubulin (1:8000, Sigma-Aldrich), rabbit anti-calnexin (1:2000, Sigma-Aldrich), rabbit anti-KIAA1107 (1:1000, PRIMM), mouse anti-AP2α (1:1000, BD Transduction Laboratories), mouse anti-AP2β (1:200, Santa Cruz), rabbit anti-FLAG (1:1000, Sigma-Aldrich), mouse anti-clathrin heavy chain (1:2000, BD Transduction Laboratories), mouse anti-synaptotagmin-1 (1:1000, Synaptic Systems), rabbit anti-synaptophysin (1:5000, Synaptic Systems), mouse anti-dynamin1 (1:1000, BD Transduction Laboratories). Membranes were washed and incubated for 1 h at room temperature with peroxidase-conjugated goat anti-mouse (1:3000; Bio-Rad) or anti-rabbit (1:5000; Bio-Rad) antibodies. Bands were revealed with the ECL chemiluminescence detection system (Thermo Scientific) and quantification of recovered immunoreactivity was performed by densitometric analysis of the fluorograms.

Subcellular fractionation and CCV purification. Subcellular fractions were prepared from 5-6 weeks old male Sprague-Dawley rat forebrain as previously described (Huttner et al., 1983). CCV-enriched fractions were prepared from 18 DIV rat neuronal cultures grown on poly-D-lysine-coated 100 mm dishes (3 x 10^6/dish). Ten dishes were homogenized in buffer A (0.1 M MES, 1 mM EGTA, 0.5 mM $MgCl_2$, pH 6.5) and protease inhibitors. The lysates were then processed by differential centrifugation coupled with D_2O-sucrose cushion centrifugation in MES buffer at pH 6.5 to stabilize the clathrin coat as in Girard et al. (2005) and CCV pellets were subjected to SDS-PAGE and Western blotting. For removal of clathrin coat, 100 µl of CCVs were diluted in 1 ml of 0.5 M Tris pH 9.0 with protease inhibitors, and rotated for 1 h at 37 °C. After centrifugation for 30 min at 120,000 x g (Beckman TLA 100.3 rotor), the pelleted stripped CCVs were resuspended in 100 µl of buffer A (Maycox et al, 1992).

Pull-down assay. p3XFLAG-KIAA1107 full length, N- and C-terminal fragments and empty vector as control were overexpressed in COS-7 and SH-SY5Y cells and purified by anti-Flag M2 Affinity gel (Sigma-Aldrich). The immunocomplexes from COS-7 cells transfection were further incubated overnight at 4 °C with either cytosolic and microsomal fraction (S2) or crude synaptosomal extracts (P2) prepared from mouse brain, or total mouse brain extracts to allow the binding of potential interacting proteins. For both cellular models, specifically bound proteins were eluted in SDS-PAGE sample buffer, subjected to SDS-PAGE on 10% polyacrylamide gels, and processed for Coomassie staining and mass spectrometry, or Western blotting.

Co-immunoprecipitation assay. Mouse brains or livers were homogenized in ice-cold buffered sucrose solution plus 100 mM NaCl and protease inhibitors and cleared by low speed centrifugation (1,000 × g for 10 min at 4 °C). The supernatant was incubated with 1% Triton X-100 for 30 min at 4 °C and then centrifuged at 58,000 rpm for 45 min. Equivalent amounts of brain or liver extract were incubated for 3 h at 4 °C with either rabbit anti-KIAA1107 or mouse anti-AP2α antibodies or rabbit/mouse control IgG (10 µg/sample) pre-coated overnight with Protein A/G-Sepharose (GE Healthcare). After extensive washes, samples were resolved by SDS–PAGE and analyzed by Western blotting.

Methyl tetrazolium salt (MTT) reduction assay

Cell viability was estimated by the MTT reduction assay, an indicator of mitochondrial activity of living cells. Primary cortical neurons from C57BL/6J mice were cultured as described above and infected with lentiviral vectors at 12 DIV.

At 17 DIV cells were washed and incubated with the MTT solution for 3 h at 37 °C (1/10 in serum-free culture medium; stock: 5 mg/ml in PBS; Sigma-Aldrich). The medium was harvested and MTT crystals were solubilized by adding DMSO (same volume as MTT medium) and incubated 15 min at dark, on a shaker. Wells were then read at 570 nm with background subtraction at 620 nm, using a Benchmark Microplate Reader, with Microplate Manager Version 5.1 Software (Bio-Rad).

Mass spectrometry (MS) analysis

Liquid chromatography–tandem MS (LC–MS/MS) analysis. Bands of interest were cut from Coomassie stained gels, reduced, alkylated and finally digested overnight with trypsin (Roche) as previously described (Matafora et al., 2009). After acidification, peptide mixtures were concentrated and desalted on homemade Stagetips μC18 (Rappsilber et al., 2003), dried in a Speed- Vac and resuspended in 10 μL of 0.1% formic acid. LC- ESI-MS/MS of 5 μL of each sample was performed on a Fourier transformed-LTQ mass spectrometer (FT-LTQ, Thermo Electron, San Jose, CA). Peptides separation was achieved on a linear gradient from 100% solvent A (5 % ACN, 0.1% formic acid) to 20% solvent B (acetonitrile, 0.1% formic acid) over 30 min and from 20% to 80% solvent B in 20 min at a constant flow rate of 0.3 μL/min on Agilent chromatographic separation system 1100 (Agilent Technologies, Waldbronn, Germany) where the LC system was connected to a 15 cm fused-silica emitter of 75 μm inner diameter (New Objective, Inc. Woburn, MA USA), packed in-house with ReproSil-Pur C18-AQ 3 μm beads (Dr. Maisch Gmbh, Ammerbuch, Germany) using a high-pressure bomb loader (Proxeon, Odense, Denmark). Survey MS scans were acquired in the FT from *m/z* 350-1650 with 100 000 resolution. The five most intense doubly and triply charged ions were automatically selected for fragmentation. Target ions already selected for the MS/MS were dynamically excluded for 60 s.

Database Searching. Tandem mass spectra were extracted by RAW2MSM ver.1.10_2007_06.14, converted into peaklist (.msm) and analyzed using Mascot (Matrix Science, London, UK; version 2.3.02) and X! Tandem (The GPM, thegpm.org; version CYCLONE (2010.12.01.1)) searching against UniProt_CP_Mouse_20131113 database (51192 entries) or UniProt_KB_ SwissProt_2013_12 database (selected for Mammalia, 66197 entries). Searches were performed by assuming as digestion enzyme trypsin, a fragment ion mass tolerance of 0.50 Da and a parent ion tolerance of 10 PPM; carbamidomethyl of cysteine was specified as a fixed modification, oxidation of methionine and acetyl of the N-terminus as variable modifications. Glu->pyro-Glu of the N-terminus, ammonia-loss of the N-terminus, gln->pyro-Glu of the N-terminus were specified in X! Tandem as variable modifications.

Criteria for protein identification. Scaffold (version Scaffold_4.4.3, Proteome Software Inc., Portland, OR) was used to validate MS/MS based peptides and protein identification. Peptide identifications were accepted if they could be established at greater than 95 % probability. Peptides Probabilities from X! Tandem were assigned by the Scaffold Local FDR algorithm. Peptide Probabilities from Mascot (Ion Score Only) were assigned by the Peptide Prophet algorithm (Keller et al, 2002) with Scaffold delta-mass correction. Protein identifications were accepted if they could be established at greater than 99 % probability and contained at least 5 identified peptides. Protein probabilities were assigned by the Protein Prophet algorithm (Nesvizhskii et al, 2003). Proteins that contained similar peptides and could not be differentiated based on MS/MS analysis alone were grouped to satisfy the principles of parsimony. Proteins sharing significant peptide evidence were grouped into clusters.

In utero electroporation (IUE)

IUE was performed as previously described (Szczurkowska et al., 2016). Briefly, E15.5 timed-pregnant CD1 mice (Charles River SRL, Italy) were anesthetized with isoflurane (induction, 4.0%; surgery, 2.0%), and the uterine horns were exposed by laparotomy. The DNA (ShRNActr or ShRNA#2 for KIAA1107 downregulation both ligated into pRNAT-U6.3/Hygro vectors (GenScript), 1.5μg/μl in water) together with the dye Fast Green (0.3 mg/ml; Sigma) was injected (3-4 μl) through the uterine wall into one of the lateral ventricles of each embryo by a 30G needle (Pic indolor, Grandate, Italy). For uniform visualization of transfected neurons and to ensure balance of the total plasmid mass in each electroporation, we co-electroporated each plasmid together with pCAGGs-IRES-EGFP. The embryo's head was carefully held between tweezer-type circular electrodes (3 mm diameter for standard electroporation or 10 mm diameter for tripolar electroporation; Nepa Gene) across the uterine wall. For the electroporation, 6 electrical pulses (amplitude, 30 V; duration, 50 ms; intervals, 1 ms) were delivered with a square-wave electroporation generator (CUY21EDIT; Nepa Gene). Then, the uterine horns were returned to the abdominal cavity, and embryos were allowed to continue their normal development.

Slice histology, image acquisition and analysis.

P7 brains were fixed by transcardial perfusion with PFA solution. Then brains were cryopreserved in 30% sucrose and sectioned coronally in 70 μm thick slices with a microtome-refrigerator (Microm HM 450 Sliding Microtome equipped with Freezing Unit Microm KS34, Thermo Scientific). Slices were counterstained with Hoechst (2,5 μg/μl; Sigma). All slices were mounted in Vectashield Mounting Medium (Vector Laboratories, Burlingame, CA). For analysis of migration and dendritic arborization, image acquisition and analysis was performed on GFP fluorescence from transfected cells. For migration analysis, images of randomly chosen cortical slices at the level of the somatosensory cortex were acquired on a Neurolucida epifluorescence microscope equipped with the software Neurolucida (MicroBrightField) and a 20X objective (NA 0.7). The contrast of the images was adjusted to enhance the fluorescence of cell bodies while attenuating the signal from neuronal processes to facilitate cell counting. 1 image was acquired per

animal. For morphology analysis, pyramidal neurons were acquired using a confocal laser-scanning microscope (TCS SP5; Leica Microsystems, Milan, Italy) equipped with a 63X immersion objective (NA 1.4). Images (1 μm thick z-stacks) were acquired and then projected on a 2D image. The settings were maintained constant for all images. 1-3 images were acquired per animal. Analysis of total branch number and length were performed with ImageJ software using the freehand line tool.

Transmission electron microscopy (TEM)

Low-density cultures of cortical neurons were infected at 12 DIV with either control shRNA or KIAA1107 shRNAs plus KIAA1107-EGFP in rescue experiments and processed for TEM. Neurons were fixed at 17 DIV with 1.2% glutaraldehyde in 66 mM sodium cacodylate buffer, post-fixed in 1% OsO4, 1.5% $K_4Fe(CN)_6$, 0.1 M sodium cacodylate, en bloc stained with 10% of uranyl acetate replacement stain (EMS) for 30 min, dehydrated, and flat embedded in epoxy resin (Epon 812, TAAB). After baking for 48 h, the glass coverslip was removed from the Epon block by thermal shock and neurons were identified by means of a stereomicroscope. Embedded neurons were then excised from the block and mounted on a cured Epon block for sectioning using an EM UC6 ultramicrotome (Leica Microsystems). Ultrathin sections (60–70 nm thick) were collected on 200-mesh copper grids (EMS) and observed with a JEM-1011 electron microscope (Jeol, Tokyo, Japan) operating at 100 kV using an ORIUS SC1000 CCD camera (Gatan, Pleasanton, CA). For each experimental condition, at least 30 images of synapses were acquired at 10,000x magnification (sampled area per experimental condition: 36 μm^2). Synaptic profile area, SV number, and distribution relative to the active zone (AZ) were determined using ImageJ. SVs were defined as vesicles with a diameter of approximately 40 nm, coated vesicles were recognized as vesicles in which the cytoplasmic surface is covered by the electrondense structure made by polyhedral lattice, endosomal structures were defined as vesicles or cisternae with a diameter >80 nm. For the 3D reconstruction, the standard TEM sample preparation protocol was followed and samples were embedded in Epon resin. Serial 60 nm-thick sections were collected on carbon-coated copper slot formvar and carbon-coated grids, and serial synaptic profiles acquired. Serial sections were aligned using the Midas of IMOD. Synapses with one single AZ, at least one docked SV and >200 total SVs were reconstructed with the software IMOD. For the analysis of synaptic ultrastructure under stimulation, primary cortical neurons were infected as described above. Infected neurons were field stimulated at 17 DIV (5 days post-infection) with a train stimulation protocol of 5 s at 40 Hz or 40 s at 5 Hz with an insulated pulse stimulator (A-M Systems). Experiments were performed in Tyrode's buffer containing 50 μM APV, 10 μM CNQX and 10 mg/ml soluble HRP. At the end of the stimulus, soluble HRP was washed out and neurons were fixed either immediately or after 2 or 20 min in 1.25% glutaraldehyde in 66 mM sodium cacodylate buffer at 37 °C. Under these conditions, we estimated a complete fixation of synapses within 1-3 s from fixative addition (Leung, 1994). After chemical fixation, neurons were washed in 0.1 M cacodylate buffer and incubated for 10 min in a solution containing 0.3 mg/ml of 3,3-diaminobenzine (DAB) in 0.1 M cacodylate buffer. Neurons were incubated in a solution containing 0.3 mg/ml of DAB + 0.003% H_2O_2 in 0.1 M cacodylate buffer until a brown substrate developed, to allow for HRP peroxidation. Neurons were then rinsed in cold distilled water, to block DAB peroxidation and post-fixed in 1% OsO_4, 1.5% $K_4Fe(CN)_6$, 0.1 M sodium cacodylate and then processed for conventional electron microscopy as described above. HRP-labeled structures were recognized thanks to the strong electrondense product reaction made by the interaction between DAB and HRP.

Live imaging experiments

Hippocampal neurons, grown onto poly-L-lysine-treated glass coverslips, were coinfected at 12 DIV with either control shRNA or KIAA1107 shRNAs and synaptophysin-pHluorin (SypHy). At 17 DIV coverslips were mounted on the stimulation chamber (Warner Instruments, Hamden, CT), immersed in Tyrode Solution (140 mM NaCl, 3 mM KCl, 2 mM $CaCl_2$, 1 mM $MgCl_2$, 10 mM HEPES-buffered to pH 7.4, 10 mM glucose) and located on the stage of an IX-81 motorized inverted epifluorescence microscope (Olympus, Hamburg, Germany). The imaging buffer was supplemented with glutamate receptor inhibitors (CNQX 10 μM; APV 50 μM; Tocris, Bristol, UK) to reduce spontaneous activity and prevent recurrent excitation during stimulation. An Hg-Xe lamp (Olympus) was used as light source with 480±20 nm excitation, 495 nm dichroic and 525±50 nm emission filters to detect the GFP (SypHy) signal and 560±40 nm excitation, 585 nm dichroic and 630±75 nm emission filters to detect the mCherry (ShRNA) signal. Time-lapses were acquired at 1 Hz for 100 s with an Orca-ER IEEE1394 CCD camera (Hamamatsu Photonics, Hamamatsu City, Japan) using an UplanSapo 60X1.35 NA oil-immersion objective (Olympus). Cells were maintained in a saline solution at room temperature through a laminar-flow perfusion and the selected field was stimulated after 10 seconds of baseline acquisition. Action potentials (AP) were evoked by passing 1-ms current pulses through platinum-iridium electrodes using an AM 2100 stimulator (AM-Systems, Carlsborg, WA). One image on mCherry channel was acquired at the beginning of each experiment to verify the presence of Cherry-tagged vectors for KIAA1107 silencing and relative control in the processes to be analyzed. Circular ROIs of 1.7 μm diameter were positioned manually at the center of each responsive synapse.

To evaluate the effects of KIAA1107 silencing on SV trafficking, a stimulation protocol of 200 APs at 5 Hz was applied. After 10 s of baseline acquisition (F_0), neurons were stimulated at 200 APs at 5 Hz; 8 min after the end of the stimulation a second stimulation was given in the presence of the clathrin-dependent endocytosis inhibitor Pitstop-2 (30 μM in DMSO, final concentration of DMSO 2% v/v; Abcam), and finally neurons were subjected to alkalinization by perfusion with 50 mM NH_4Cl (F_{max}). Images were analyzed using the eXcellence software (Olympus). The total

increase in the fluorescence signal (ΔF) was calculated by subtracting F_0 and the ΔF was normalized to the fluorescence value obtained by alkalization of the entire vesicle pool using NH_4Cl (ΔF_{max}). The time constant of endocytosis (τ endo) and the percent of retrieved SVs (a) were calculated by fitting the post-stimulus decay with a single-exponential function. To get release rates, traces recorded during stimulation were individually fitted to obtain individual time constants of release (τ release). N refers to the number of coverslips analyzed from 3-4 different preparations. Data were collected from 20-40 boutons per coverslip.

Electrophysiology

Patch-clamp recordings. Whole-cell patch-clamp recordings were performed on primary cultures of hippocampal neurons grown as autaptic cells as previously described (Valente et al., 2016). Patch pipettes, prepared from thin-borosilicate glass (Hilgenberg, Mansfield, Germany), were pulled and fire-polished to a final resistance of 2-4 MΩ when filled with standard internal solution. Evoked postsynaptic currents (eEPSCs) were recorded using a double EPC-10 amplifier (HEKA Electronic, Lambrecht, Germany). For recordings, cells were maintained in a standard external solution containing (in mM): 140 NaCl, 2 $CaCl_2$, 1 $MgCl_2$, 4 KCl, 10 glucose, 10 HEPES (pH 7.3 with NaOH). To record eEPSCs, where otherwise not indicated, D-(-)-2-amino-5-phosphonopentanoic acid (D-AP5 50 μM; Tocris) and bicuculline methiodide (30 μM; Tocris) were added to the Tyrode external solution to block N-methyl-D-aspartate (NMDA) and $GABA_A$Rs, respectively. The standard internal solution was (in mM): 126 KGluconate, 4 NaCl, 1 $MgSO_4$, 0.02 $CaCl_2$, 0.1 BAPTA, 15 glucose, 5 HEPES, 3 ATP, 0.1 GTP (pH 7.2 with KOH). All experiments were performed at room temperature (22-24 °C). Neurons were voltage-clamped at -70 mV. Unclamped APs were evoked by a brief depolarization of the cell body to +40 mV for 0.5 ms at 0.1 Hz. eEPSCs were acquired at 10-20 kHz sample frequency and filtered at half the acquisition rate with an 8-pole low-pass Bessel filter. Recordings with leak currents >100 pA or series resistance >20 MΩ were discarded. Data acquisition was performed using PatchMaster programs (HEKA Elektronic, Lambrecht, Germany). eEPSCs were inspected visually, and only those that were not contaminated by spontaneous activity were considered. To calculate the peak current during an isolated stimulus or a train of stimuli, we first subtracted an averaged trace containing the stimulus artifact and the AP current, but lacking any discernable synaptic current (i.e. synaptic failures). Such traces were easily identified toward the end of a train of stimuli, when synaptic depression was maximal. These traces were averaged and scaled to the peak Na^+ current contaminating the eEPSCs.

Short-term plasticity paradigms. To analyze paired-pulse ratio (PPR), two brief depolarizing pulses (0.5 ms at 40 mV) were applied to autaptic neurons with a time intervals of 50 ms. For each couple of eEPSCs, PPR was calculated as the ratio I2/I1, where I1 and I2 are the amplitudes of the eEPSCs evoked by the conditioning (1) and test (2) stimuli, respectively. To correctly estimate the amplitude of I2, the baseline of I2 was defined as the final value of the decay phase of I1 and the amplitude of I2 was calculated by subtracting the residual amplitude of I1 from the peak value of I2. For the evaluation of the synaptic responses during tetanic stimulation, the time interval was shorter than the time needed for an eEPSC to return to baseline, so eEPSCs overlapped partially. Then, to correctly estimate the EPSC amplitude, the baseline of each event was defined as the final value of the decay phase of the preceding eEPSC; then, the amplitude of $(eEPSC)_n$ was calculated by subtracting the residual amplitude of $(eEPSCs)_{n-1}$ from its peak value. For the evaluation of post-tetanic potentiation (PTP), autaptic neurons were depolarized with short-trains of stimuli (2 s at 40 Hz). The peak PTP was determined by measuring the maximal amplitude of the eEPSCs, usually obtained 10 or 20 s after the end of the train.

Cumulative eEPSC amplitude analysis. The size of the readily releasable pool of synchronous release (RRP) and the probability that any given SV in the RRP will be released (Pr) were calculated using the cumulative amplitude analysis (Schneggenburger et al., 2002). The cumulative amplitude plot was determined by summing up peak EPSC amplitudes during 80 repetitive stimuli applied at 40 Hz. This analysis assumes that depression during the steady-state phase is limited by a constant recycling of SVs and an equilibrium occurs between released and recycled SVs and that Pr during the train approaches the 1 value (Schneggenburger et al., 1999). The number of data points for the linear fitting of the steady-state phase was evaluated by calculating the best fit including the maximal number of data points starting from the last data point (i.e., from the 80^{th} eEPSC). The cumulative amplitude profiles of the last 30-40 data points were fitted by linear regression and backextrapolated to time 0. The intercept with the Y-axis gave the RRP and the ratio between the amplitude of the first eEPSC (I1) and RRP yielded the Pr.

SUPPLEMENTAL REFERENCES:

Adler, J., Parmryd, I. (2010). Quantifying colocalization by correlation: the Pearson correlation coefficient is superior to the Mander's overlap coefficient. *Cytometry A* 77, 733-742

Daum, J.R., Wren, J.D., Daniel, J.J., Sivakumar, S., McAvoy, J.N., Potapova, T.A., Gorbsky, G.J. (2009). Ska3 is required for spindle checkpoint silencing and the maintenance of chromosome cohesion in mitosis. *Curr. Biol.* 19, 1467-1472

Huttner, W.B., Schiebler, W., Greengard, P. and De Camilli, P. (1983). Synapsin I (protein I), a nerve terminal-specific phosphoprotein. III. Its association with synaptic vesicles studied in a highly purified synaptic vesicle preparation. *J Cell Biol* 96, 1374-1388

Keller, A., Nesvizhskii, A.I., Kolker, E., Aebersold, R. (2002). Empirical statistical model to estimate the accuracy of peptide identifications made by MS/MS and database search. *Anal Chem* 74, 5383-5392

Gandhapudi, S.K., Tan, C., Marino, J.H., Taylor, A.A., Pack, C.C., Gaikwad, J., Van De Wiele, C.J., Wren, J.D., and Teague, T.K. (2015). IL-18 acts in synergy with IL-7 to promote ex vivo expansion of T lymphoid progenitor cells. *J. Immunol.* 194, 3820-3828

Girard, M., Allaire, P.D., Blondeau, F., and McPherson, P.S. (2005). Isolation of clathrin-coated vesicles by differential and density gradient centrifugation. *Curr. Protoc. Cell Biol.* Chapter 3, Unit 3. 13

Leung, A. (1994). *Fixation. In "Laboratory histopathology: a complete reference".* AE Woods and RC Ellis eds, Churchill Livingstone, New York.

Lupu, C., Zhu, H., Popescu, N.I., Wren, J.D., Lupu, F. (2011). Novel protein ADTRP regulates TFPI expression and function in human endothelial cells in normal conditions and in response to androgen. *Blood* 118, 4463-4471

Matafora, V., D'Amato, A., Mori, S., Blasi, F., Bachi, A. (2009). Proteomics analysis of nucleolar SUMO-1 target proteins upon proteasome inhibition. *Mol Cell Proteomics* 8, 2243-2255

Maycox, P.R., Link, E., Reetz, A., Morris, S.A., and Jahn, R. (1992). Clathrin-coated vesicles in nervous tissue are involved primarily in synaptic vesicle recycling. *J. Cell Biol.* 118, 1379-1388

Nesvizhskii, A.I., Keller, A., Kolker, E., Aebersold, R. (2003). A statistical model for identifying proteins by tandem mass spectrometry. *Anal Chem* 75, 4646-4658

Pfaffl, M.W. (2001). A new mathematical model for relative quantification in real-time RT-PCR. *Nucleic Acids Res* 29, e45

Piccini, A., Perlini, L.E., Cancedda, L., Benfenati, F. and Giovedì, S. (2015). Phosphorylation by PKA and Cdk5 mediates the early effects of Synapsin III in neuronal morphological maturation. *J Neurosci* 35, 13148-13159

Rappsilber, J., Ishihama, Y., Mann, M. (2003). Stop and go extraction tips for matrix-assisted laser desorption/ionization, nanoelectrospray, and LC/MS sample pretreatment in proteomics. *Anal Chem* 75, 663-670

Schneggenburger, R., Sakaba, T., Neher, E. (2002). Vesicle pools and short-term synaptic depression: lessons from a large synapse. *Trends Neurosci* 25, 206-212

Valente, P., Castroflorio, E., Rossi, P., Fadda, M., Sterlini, B., Cervigni, R.I., Prestigio, C., Giovedì, S., Onofri, F., Mura, E., et al. (2016). PRRT2 is a key component of the Ca^{2+}-dependent neurotransmitter release machinery. *Cell Reports* 15, 117-131

Vandesompele, J., De Preter, K., Pattyn, F., Poppe, B., Van Roy, N., De Paepe, A., Speleman, F. (2002). Accurate normalization of real-time quantitative RT-PCR data by geometric averaging of multiple internal control genes. *Genome Biol* 3: research0034

	Predicted Assn.	# shared rels	Score
Cellular/anatomical structures	hippocampal neurons	12	96
	dendrites	6	70
	gyrus	6	52
	compact myelin	4	49
	basal body	5	42
	voltage-gated potassium channels	4	39
	myelin sheath	6	38
	sensory neurons	6	32
	retinal ganglion	7	32
	neurofilament	7	28
	cortical neurons	6	27
	cerebellum	11	26
	optic nerve	8	25
	myelin oligodendrocyte glycoprotein	4	24
Diseases	Schizophrenia	9	100
	Autism	6	55
	ciliopathy	4	52
	Epilepsy	8	36
Phenotypes	synaptic transmission	9	105
	cilium assembly	6	80
	synaptic vesicle recycling	4	73
	synaptic proteins	7	66
	synaptic vesicle endocytosis	4	65
	neurite outgrowth	7	39
	oligodendrocyte differentiation	4	38
	neurotransmitter release	5	33
	synaptic vesicles	7	32
	synaptic vesicle exocytosis	3	28
	myelination	6	26
	N-ethylmaleimide-sensitive factor	4	26
	excitatory synaptic transmission	4	25
	postsynaptic density	4	24
	long-term potentiation	6	23

FIGURE S1

Figure S1 (related to Fig. 1)
GAMMA predicted phenotypes, diseases and cellular/anatomical relevance for KIAA1107
GAMMA first identified highly correlated genes via an analysis of public microarray datasets. Using a guilt-by-association approach, the 40 genes most highly correlated with KIAA1107 were analyzed with literature-mining software for significant associations. # Shared Rels shows how many out of the 40 genes are associated with each term in MEDLINE. The "Score" field reflects an enrichment of the number of observed connections in the literature network over the number of expected connections for a random network with the same connectivity.

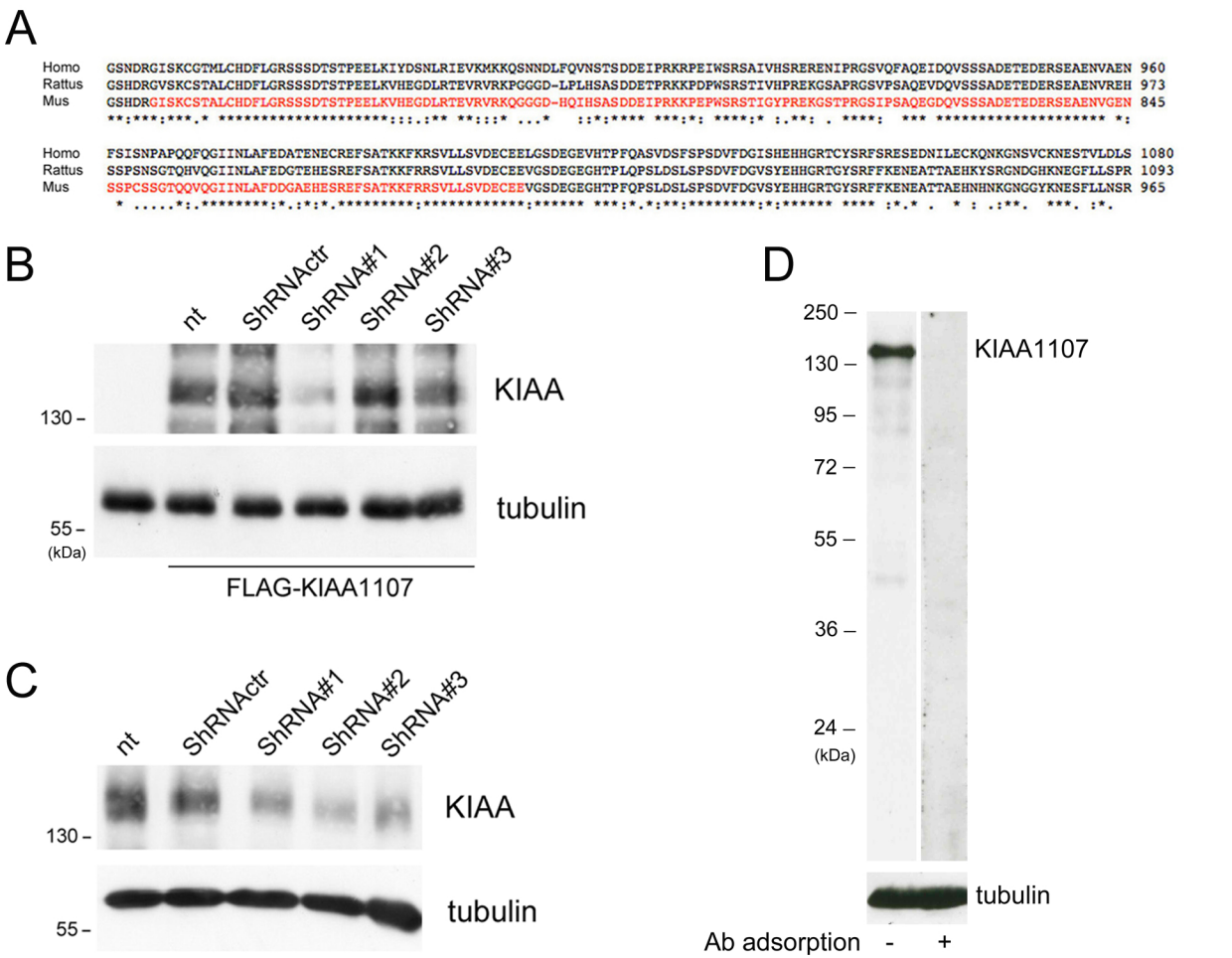
A
Homo GSNDRGISKCGTMLCHDFLGRSSSDTSTPEELKIYDSNLRIEVKMKKQSNNDLFQVNSTSDDEIPRKRPEIWSRSAIVHSRERENIPRGSVQFAQEIDQVSSSADETEDERSEAENVAEN 960
Rattus GSHDRGVSKCSTALCHDFLGRSSSDTSTPEELKVHEGDLRTEVRVRKPGGGD-LPLHSASDDETPRKKPDPWSRSTIVHPREKGSAPRGSVPSAQEVDQVSSSADETEDERSEAENVREH 973
Mus GSHDRGISKCSTALCHDFLGRSSSDTSTPEELKVHEGDLRTEVRVRKQGGGD-HQIHSASDDEIPRKKPEPWSRSTIGYPREKGSTPRGSIPSAQEGDQVSSSADETEDERSEAENVGEN 845
Homo FSISNPAPQQFQGIINLAFEDATENECREFSATKKFKRSVLLSVDECEELGSDEGEVHTPFQASVDSFSPSDVFDGISHEHHGRTCYSRFSRESEDNILECKQNKGNSVCKNESTVLDLS 1080
Rattus SSPSNSGTQHVQGIINLAFEDGTEHESREFSATKKFRRSVLLSVDECEEVGSDEGEGHTPLQPSLDSLSPSDVFDGVSYEHHGRTGYSRFFKENEATTAEHKYSRGNDGHKNEGFLLSPR 1093
Mus SSPCSSGTQQVQGIINLAFDDGAEHESREFSATKKFRRSVLLSVDECEEVGSDEGEGHTPFQPSLDSLSPSDVFDGVSYEHHGRTGYSRFFKENEATTAEHNHNKGNGGYKNESFLLNSR 965
B
nt
ShRNActr
ShRNA#1
ShRNA#2
ShRNA#3
130 –
KIAA
55 –
(kDa)
tubulin
FLAG-KIAA1107
C
nt
ShRNActr
ShRNA#1
ShRNA#2
ShRNA#3
130 –
KIAA
55 –
tubulin
D
250 –
130 –
95 –
72 –
55 –
36 –
24 –
(kDa)
KIAA1107
tubulin
Ab adsorption - +
E
ShRNA#2
KIAA
ShRNA#2/KIAA

FIGURE S2

Figure S2 (related to Fig. 1)
Experimental tools for the study of KIAA1107
(A) Sequence alignment of human, rat and mouse KIAA1107 regions encompassing the epitope (aa 732-894 of the mouse sequence, red) used for raising the KIAA1107 antibody. Several consensus sequences accounting for the specificity of KIAA1107 antibody in the three species are present (* identity; : strong similarity; . weak similarity). Ref ID: Kiaa1107 *Homo Sapiens* 1354 aa, ref|NP_056052.2; Btbd8 *Rattus Novegicus* 1367 aa, ref D4A0X3; Kiaa1107 *Mus Musculus* 1088 aa, ref|NP_001007575.2. **(B,C)** Specificity of anti-KIAA1107 antibody and KIAA1107 downregulation. ShRNA#1-3 or control ShRNA (ShRNActr) were cotransfected with mouse FLAG-KIAA1107 in COS-7 cells using Lipofectamine2000 **(B)** or nucleofected by Amaxa before plating in mouse primary cortical neurons **(C)**. After 48 h for COS-7 cells and 5 days for primary neurons, cell lysates were analyzed by Western blotting and probed with anti-KIAA1107 antibodies. In COS-7 cells, only ShRNA#1, designed against the coding sequence, was effective in downregulating overexpressed KIAA1107, whereas virtually all ShRNAs (including ShRNA#2 and #3 designed against the 3'-UTR) were able to knockdown endogenous KIAA1107 in neurons. ShRNActr did not affect KIAA1107 expression. nt, untreated cells. βIII tubulin immunoreactivity was used as loading control. **(D)** Pre-adsorption assays. Anti-KIAA1107 primary antibody was pre-adsorbed with a 10-fold molar excess of the immunizing peptide (His-tag fusion protein) by an overnight incubation at 4 °C. Western blots were performed in parallel on mouse brain total homogenate using either untreated (-) or pre-adsorbed (+) anti-KIAA1107 primary antibody. βIII tubulin immunoreactivity was used as loading control. **(E)** Representative images of 5 days *in vitro* (DIV) cortical neurons nucleofected by Amaxa before plating with ShRNA#2 (red) and immunostained with anti-KIAA1107 antibodies (green). Note the absence of the green fluorescence immunoreactivity in neurons transfected with ShRNAs for KIAA1107. Scale bar, 50 μm.

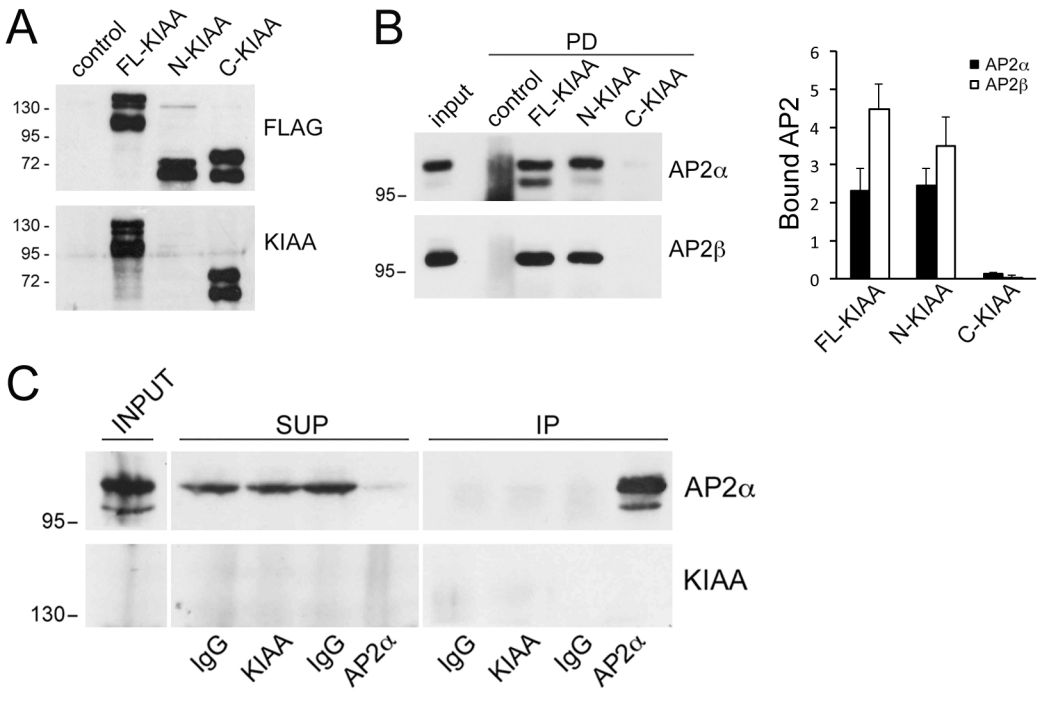
A
control
FL-KIAA
N-KIAA
C-KIAA
130-
95-
72-
FLAG
130-
95-
72-
KIAA
B
PD
input
control
FL-KIAA
N-KIAA
C-KIAA
95-
AP2α
95-
AP2β
Bound AP2
AP2α
AP2β
6
5
4
3
2
1
0
FL-KIAA
N-KIAA
C-KIAA
C
INPUT
SUP
IP
95-
AP2α
130-
KIAA
IgG
KIAA
IgG
AP2α
IgG
KIAA
IgG
AP2α

FIGURE S3

Figure S3 (related to Fig. 2)
Specificity of AP2-KIAA1107 interaction
(A,B) Pulldown assays with FLAG-tagged constructs. **(A)** FLAG-tagged full-length KIAA1107 (FL-KIAA), N-terminal fragment (N-KIAA), C-terminal fragment (C-KIAA) or FLAG alone (control) were expressed in COS-7 cells and purified by anti-FLAG M2 affinity gel. Immunoblotting with anti-FLAG (top) and anti-KIAA1107 (bottom) antibodies show the similar expression levels of the FLAG-tagged KIAA1107 constructs in COS-7 cells. The anti-KIAA1107 antibody correctly recognizes only the C-terminal region. **(B)** Purified FLAG-tagged full-length KIAA1107 (FL-KIAA), N-terminal fragment (N-KIAA), C-terminal fragment (C-KIAA) or FLAG alone (control) on anti-FLAG M2 affinity gel were incubated with mouse brain extracts. After pulldown (PD), pellets were subjected to immunoblotting together with aliquots of the starting material (input) using antibodies for AP2α and AP2β. *Left:* Representative immunoblots are shown. The same membranes were stripped and re-probed for AP2α and AP2β. *Right:* Densitometric quantification of AP2α and AP2β immunoreactive signals in the pulldown samples, normalized to the binding to FLAG control (means ± SEM of n=3 independent experiments). **(C)** Mouse liver extracts were subjected to immunoprecipitation (IP) assays with anti-KIAA1107 polyclonal antibodies, anti-AP2α monoclonal antibodies or control IgGs. Equal aliquots of the starting material (INPUT) and of the supernatants (SUP) together with IP samples were subjected to immunoblotting with antibodies to KIAA1107 and AP2α. AP2 was efficiently immunoprecipitated only with anti-AP2 antibodies, but not with anti-KIAA1107 antibodies.

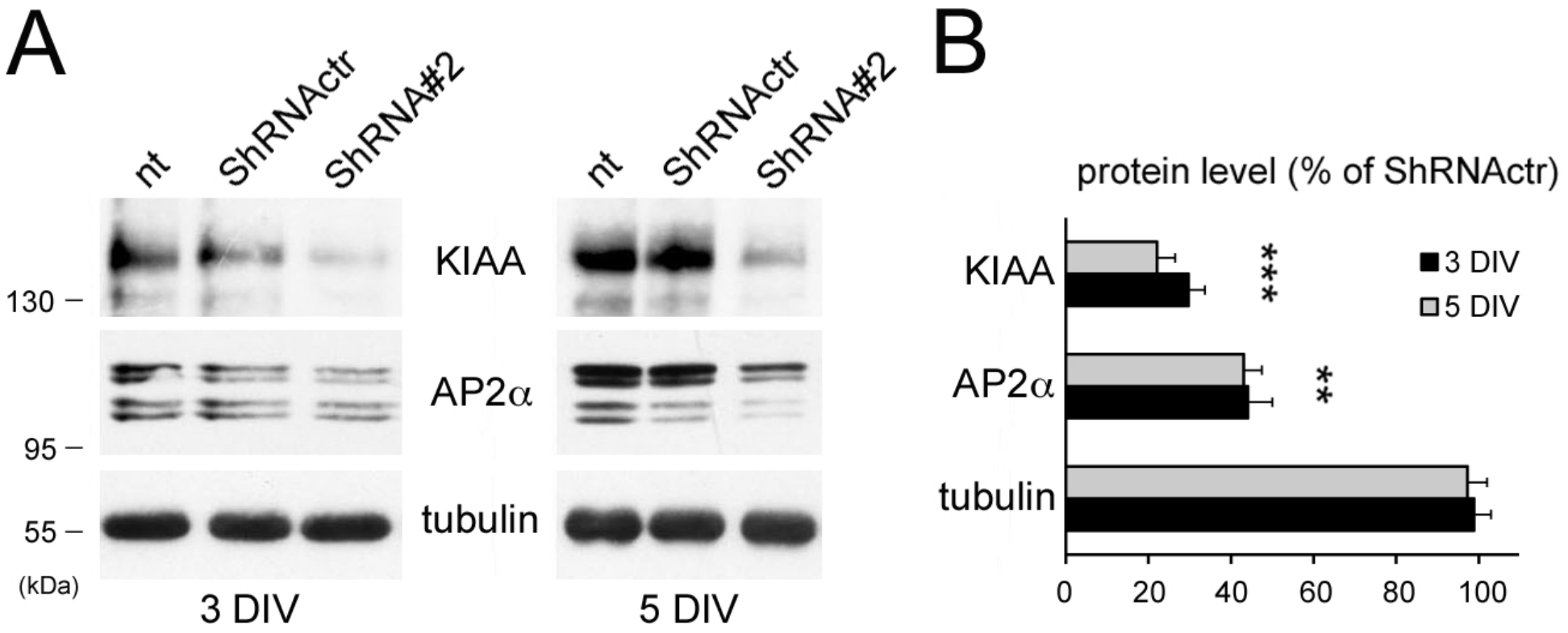
A
nt
ShRNActr
ShRNA#2
nt
ShRNActr
ShRNA#2
KIAA
AP2α
tubulin
130 –
95 –
55 –
(kDa)
3 DIV
5 DIV
B
protein level (% of ShRNActr)
KIAA
AP2α
tubulin
***
**
3 DIV
5 DIV
0
20
40
60
80
100

FIGURE S4

Figure S4 (related to Fig. 4)

Decreased expression levels of AP2α in KIAA1107-silenced neurons at early developmental stages

(A) Primary cortical neurons were nucleofected by Amaxa before plating with control ShRNA (ShRNActr) or ShRNA#2 and total cell lysates were analyzed by Western blotting at 3 and 5 DIV with antibodies specific for KIAA1107 and AP2α. Representative immunoblots are shown. nt, non-treated neurons. βIII tubulin immunoreactivity was used as loading control. **(B)** Densitometric analysis of the immunoreactivity. The expression levels of the various proteins in KIAA1107-silenced neurons are given in percentage of the respective levels in ShRNActr-treated neurons (means ± SEM of n=3 independent experiments). Statistical analysis was performed using the unpaired Student's *t*-test, **p<0.01, ***p<0.001 vs ShRNActr neurons.

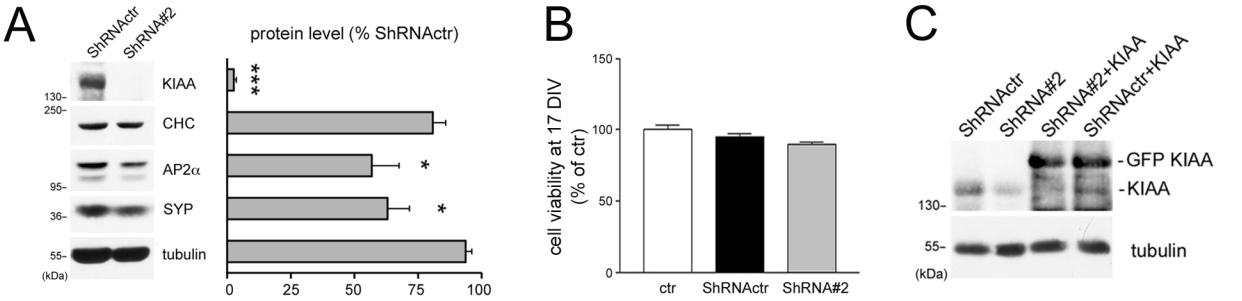
A
ShRNActr
ShRNA#2
protein level (% ShRNActr)
KIAA
CHC
AP2α
SYP
tubulin
130–
250–
95–
36–
55–
(kDa)
***
*
*
0
25
50
75
100
B
cell viability at 17 DIV
(% of ctr)
150
100
50
0
ctr
ShRNActr
ShRNA#2
C
ShRNActr
ShRNA#2
ShRNA#2+KIAA
ShRNActr+KIAA
-GFP KIAA
-KIAA
130–
55–
(kDa)
tubulin

FIGURE S5

Figure S5 (related to Fig. 5)
Silencing efficiency and neuronal viability
(A) KIAA1107 knockdown by viral infection. Cortical neurons were transduced at 12 DIV with lentiviral vectors coding for either control ShRNA (ShRNActr) or ShRNA#2 and analyzed by Western blotting at 17 DIV with antibodies specific to KIAA1107, CHC, AP2α, SYP. *Left:* a representative immunoblot is shown. βIII tubulin immunoreactivity was used as loading control. *Right:* Densitometric analysis of the immunoreactivity. The expression levels of the various proteins in KIAA1107-KD neurons are given in percentage of the respective levels in ShRNActr-treated neurons (means ± SEM of n=4 independent experiments). Statistical analysis was performed using the unpaired Student's *t*-test, *$p<0.05$, ***$p<0.001$ vs ShRNActr neurons. **(B)** Cell viability measured by the MTT assay analyzed at 17 DIV in uninfected (ctr) neurons or in neurons infected at 12 DIV with either ShRNActr or ShRNA#2. Data are expressed as means ± SEM of n=4 independent experiments. Statistical analysis was performed using one-way ANOVA/Bonferroni's multiple comparison test. **(C)** Representative immunoblot showing the specificity of ShRNA#2 in downregulating endogenous KIAA1107 levels in transduced cortical neurons at 17 DIV and the overexpression of EGFP-KIAA1107 construct intrinsically resistant to ShRNA#2 used in rescue experiments. βIII tubulin immunoreactivity was used as loading control.

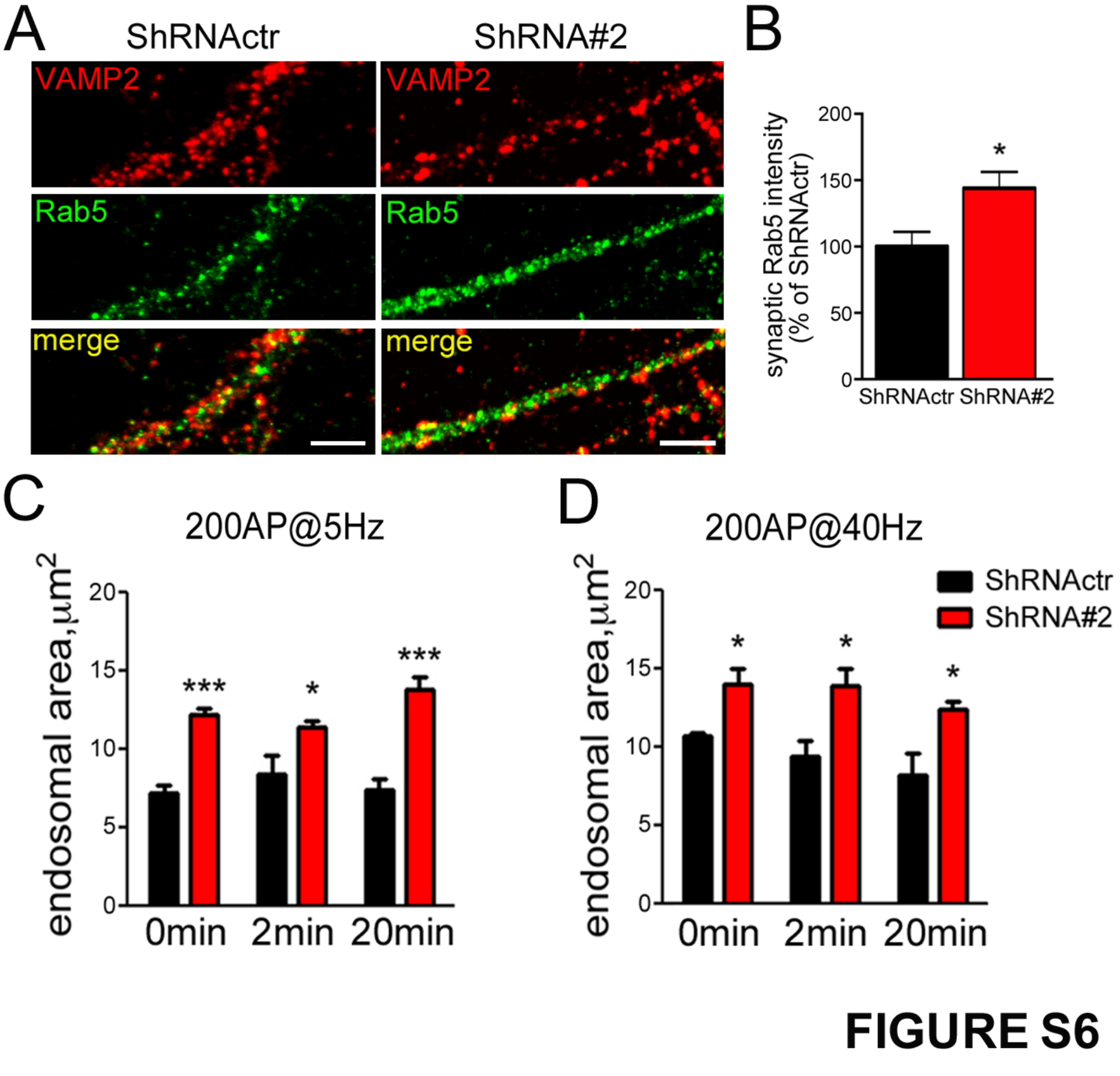
A
ShRNActr
ShRNA#2
VAMP2
VAMP2
Rab5
Rab5
merge
merge
B
synaptic Rab5 intensity
(% of ShRNActr)
200
150
100
50
0
*
ShRNActr ShRNA#2
C
200AP@5Hz
endosomal area,μm2
20
15
10
5
0
***
*
***
0min 2min 20min
D
200AP@40Hz
ShRNActr
ShRNA#2
endosomal area,μm2
20
15
10
5
0
*
*
*
0min 2min 20min

FIGURE S6

Figure S6 (related to Figs. 5 and 6)
Increased size of endosome-like structures at KIAA1107-silenced synapses
(A) Representative confocal images of synapses from cortical neurons (17 DIV) transduced with either ShRNActr or ShRNA#2 and immunostained with anti-VAMP2 (red) and anti-Rab5 (green) antibodies. Scale bars, 5 μm. **(B)** Intensity values for Rab5 signal at VAMP2-positive puncta in control (black bar) and KIAA1107-silenced (red bar) synapses. Data are means ± SEM from n=3 independent preparations. 300 synapses have been counted for each preparation. *p<0.05 vs ShRNActr, unpaired Student's *t*-test. **(C,D)** Morphometric analysis of the area of the endosome-like structures in control (black bars) and KIAA1107-KD (red bars) neurons after train stimulation at 5 **(C)** and 40 **(D)** Hz (200 APs). Data are reported as mean (± SEM) endosomal areas observed immediately after the stimulus (0 min) and after 2 or 20 min of recovery, respectively. n=150 and n=120 images per genotype for the 5 and 40 Hz protocols, respectively, from n=4 independent preparations. *p<0.05, ***p<0.001 across genotype, two-way ANOVA/Bonferroni's multiple comparison test.

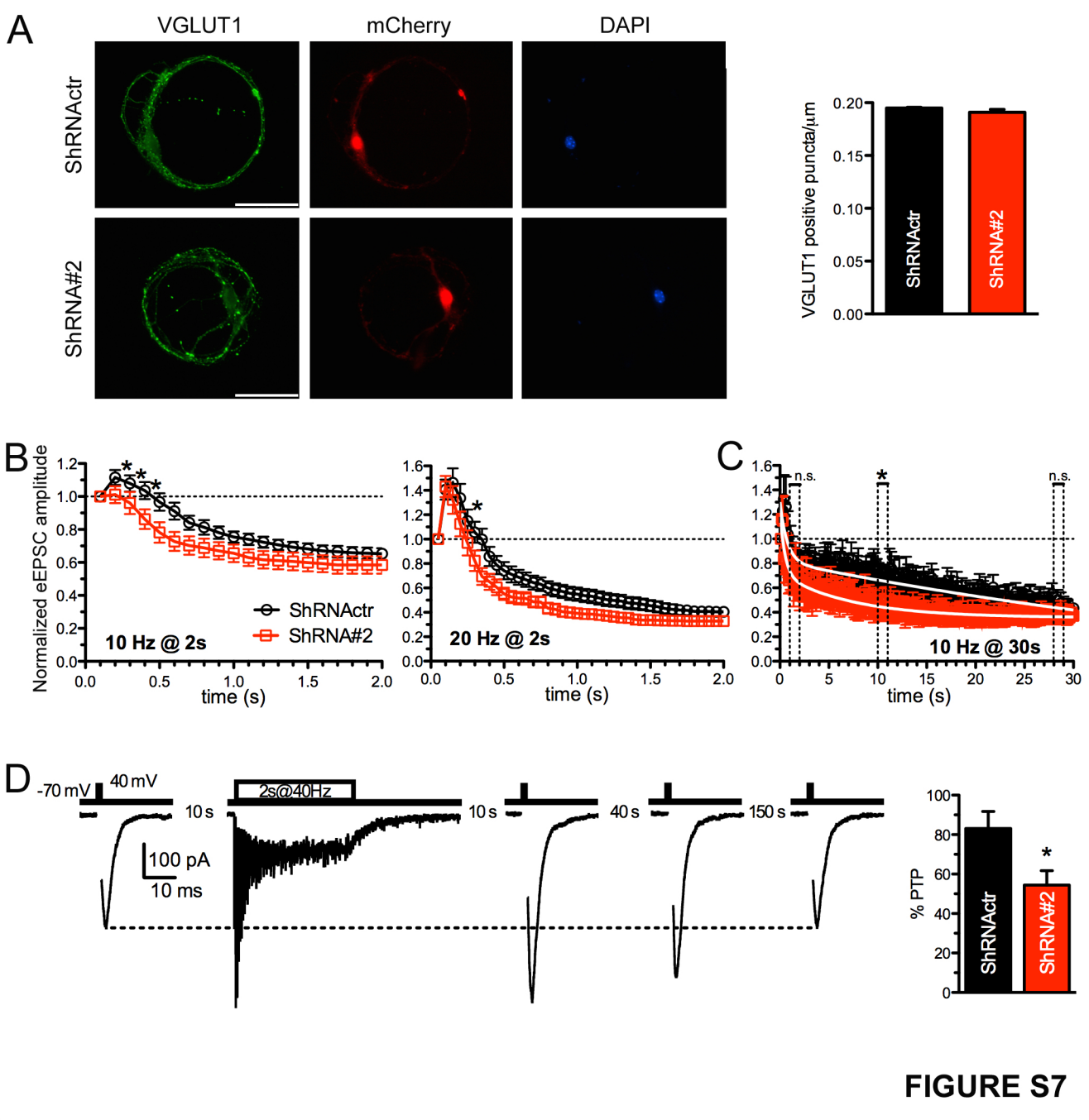
A
VGLUT1
mCherry
DAPI
ShRNActr
ShRNA#2
VGLUT1 positive puncta/μm
0.20
0.15
0.10
0.05
0.00
ShRNActr
ShRNA#2
B
Normalized eEPSC amplitude
1.2
1.0
0.8
0.6
0.4
0.2
0.0
*
*
*
ShRNActr
ShRNA#2
10 Hz @ 2s
0.0
0.5
1.0
1.5
2.0
time (s)
1.6
1.4
1.2
1.0
0.8
0.6
0.4
0.2
0.0
*
20 Hz @ 2s
0.0
0.5
1.0
1.5
2.0
time (s)
C
1.6
1.4
1.2
1.0
0.8
0.6
0.4
0.2
0.0
n.s.
*
n.s.
10 Hz @ 30s
0
5
10
15
20
25
30
time (s)
D
-70 mV
40 mV
10 s
2s@40Hz
10 s
40 s
150 s
100 pA
10 ms
% PTP
100
80
60
40
20
0
*
ShRNActr
ShRNA#2

FIGURE S7

Figure S7 (related to Fig. 7)
Response of KIAA1107-silenced neurons to high frequency stimulation
(A) *Left:* Representative images of autaptic hippocampal neurons transduced with either ShRNActr or ShRNA#2 (mCherry) and stained with an anti-VGLUT1 antibody. Scale bars, 50 μm. *Right:* Quantitative analysis of the density of VGLUT1-positive puncta. Values are expressed as means ± SEM (n=30 for both control and KIAA1107-silenced neurons). **(B,C)** Mean (± SEM) normalized values of eEPSC amplitude showing the time course of synaptic facilitation and depression in autaptic neurons transduced with either ShRNActr (black) or ShRNA#2 (red) and stimulated with 2-s trains at 10 (left) or 20 (right) Hz **(B)** or with 30-s trains at 10 Hz **(C)** (2 s at 10 Hz: ShRNActr n=32, ShRNA#2 n=17; 2 s at 20 Hz: ShRNActr n=34, ShRNA#2 n=22; 30 s at 10 Hz: ShRNActr n=8, ShRNA#2, n=7). **(D)** Silencing of KIAA1107 decreases post-tetanic potentiation (PTP). *Left:* Representative recordings of eEPSCs evoked before and 10, 40 and 150 s after tetanic stimulation (2 s at 40 Hz) in autaptic neurons transduced with ShRNActr. *Right:* Mean (± SEM) percentages of PTP in autaptic control (black bar, n=32) or KIAA1107-silenced (red bar, n=28) neurons. *p<0.05, unpaired Student's *t*-test or Mann–Whitney U-test. In all graphed currents, stimulation artifacts were blanked for clarity.